Absolute measurements of the free-fall acceleration g in Catania and Etna volcano

G. D'Agostino[(1)], *A. Germak*[(1)], *C. Origlia*[(1)],
C. Del Negro[(2)], *F. Greco*[(2)], *A. Sicali*[(2)], *S. Dorizon*[(3)]

Absolute Measurements of the Free-Fall Acceleration g in Catania and Etna Volcano

T.R. 17/2009 September 2009

(1) *Istituto Nazionale di Ricerca Metrologica* – Torino
(2) *Istituto Nazionale di Geofisica e Vulcanologia* – Catania
(3) *Ecole et Observatoire des Sciences et de la Terre* – Strasbourg

I.N.RI.M. TECHNICAL REPORT

ABSTRACT

The work hereafter described was carried out on July 2009 by the *Istituto Nazionale di Ricerca Metrologica* (INRIM) of Turin (Italy) in the framework of a cooperation with the *Istituto Nazionale di Geofisica e Vulcanologia* (INGV) – Catania Section.

The experimental results of absolute measurements of the free-fall acceleration *g* carried out at Catania and Etna Volcano are reported. Gravity measurements were performed with the transportable absolute gravimeter IMGC-02.

Il lavoro descritto in seguito è stato svolto nel mese di luglio 2008 *dall'Istituto Nazionale di Ricerca Metrologica* (INRIM) di Torino nell'attività di cooperazione con l'*Istituto Nazionale di Geofisica e Vulcanologia* (INGV) – Sezione di Catania.

Si riportano i risultati sperimentali delle misure assolute dell'accelerazione di caduta libera *g* eseguite in Catania e sul vulcano Etna. Le misure sono state effettuate con il gravimetro assoluto trasportabile IMGC-02.

INDEX

1 INTRODUCTION

The measurement of the free-fall acceleration, *g*, has been performed with the gravimeter IMGC-02. The apparatus (fig.1) is developed by INRIM /1/, and derives from that one previously realized in collaboration with the Bureau International des Poids et Mesures in Sèvres (BIPM) /2/.

Several improvements characterize the IMGC-02, among them there is the automation of the instrument which allows to perform the measurement during the night, when the disturbance due to the environmental noise is minimum.

All the measurement sessions have been recorded and stored in data files for post-processing. If necessary, these files are delivered for future revision or checking. The software was developed and tested by INRIM.

Figure 1. Picture of the absolute gravimeter IMGC-02

2 THE IMGC ABSOLUTE GRAVIMETER

2.1 Measurement method

The free-fall acceleration *g* is measured by tracking the vertical trajectory of a test-body subjected to the gravitational acceleration. The IMGC-02 adopts the *symmetric rise and falling* method, where both the rising and falling trajectories of the test-body are recorded. The raw datum consists in an array where each element represents the time correspondent to the passage of the test-body through equally spaced levels (or stations). A model function derived from the equation of motion is fitted to the raw datum in a least-squares adjustment. One of the parameters of the model is the acceleration experienced by the test-body during its flight. A *measurement session* consists of about 2000 launches. To assure the evaluated measurement uncertainty, the *g* value is obtained by averaging those launches which fulfill accepting criteria.

2.2 Apparatus

A schematic layout of the apparatus is showed in fig. 2.1. The basic parts of the instrument are a Mach-Zehnder interferometer /3/ and a long-period (about 20 s) seismometer. The wavelength of a iodine stabilised He-Ne laser is used as the length standard. The inertial mass of a seismometer supports a cube-corner reflector, which is the reference mirror of the interferometer. The moving mirror of the interferometer is also a cube-corner retro-reflector and is directly subjected to the free falling motion. It is thrown vertically upwards by means of a launch pad in a vacuum chamber (1×10^{-3} Pa). Interference fringes emerging from the interferometer are detected by a photo-multiplier. The output signal is sampled by a high-speed waveform digitizer synchronized to a Rb oscillator, used as the time standard. Equally spaced stations are selected by counting a constant integer number of interference fringes (at present 1024); in particular consecutive stations are separated by a distance $d = 1024 \cdot \lambda/2$, being λ the wavelength of the laser radiation.

The so called *local fit method* is used to time the interference signal /4/. In particular the time is computed by fitting the equation model of the interference of monochromatic waves to the interference fringe correspondent to the selected station. The space-time coordinates are processed in a least-squares algorithm, where a suitable model function is fitted to the trajectory. Each throw gives an estimate of the *g* value.

A personal computer manages the instrument. The pad launch is triggered only if the system is found to be ready. In particular the software checks the pad launch state (loaded or unloaded) and the laser state (locked or unlocked). Environmental parameters such as the local barometric pressure and the temperature are acquired and stored for each launch.

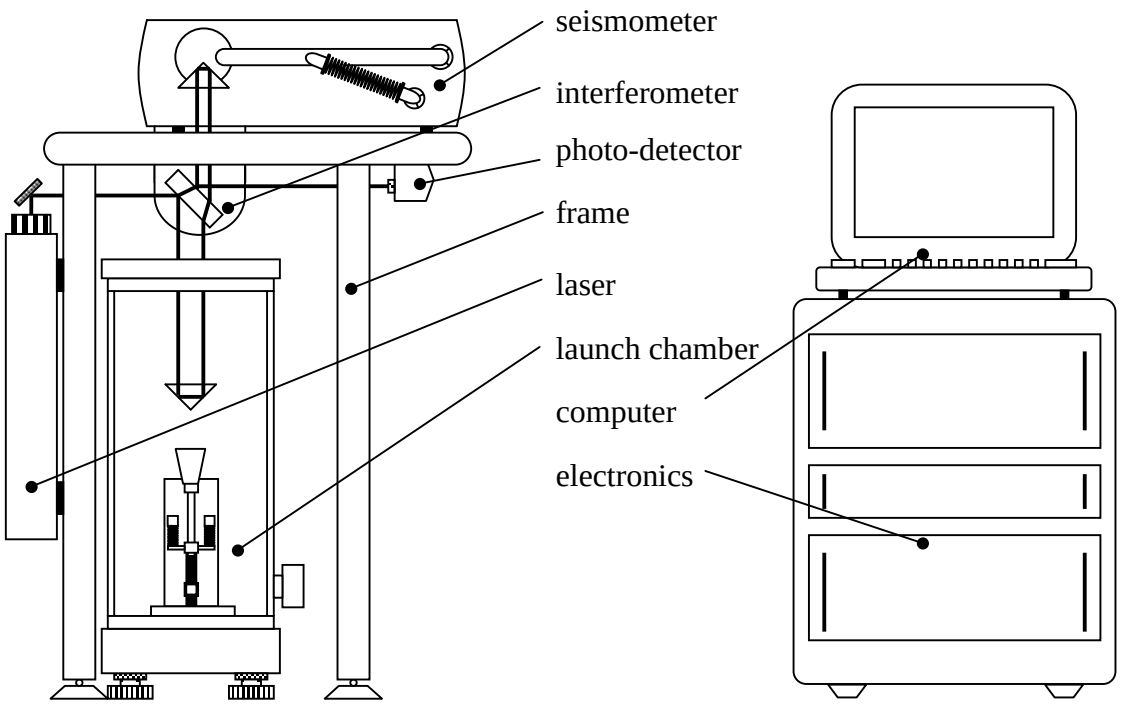

Figure 2.1. Schematic layout of the IMGC-02 Absolute Gravimeter

The software used includes (i) the manager *GravisoftM* (fig. 2.2) for driving the instrument and storing the measurement data and (ii) the post-processing *GravisoftPP* (fig. 2.3) for elaborating the data-files. These programs were developed and tested on the LabVIEW® platform.

Geophysical corrections are applied: (i) the Earth tides and Ocean loading are computed with the ETGTAB (version 3.10 19950123 Fortran 77), (ii) the polar motion correction is computed starting from the daily pole coordinates x and y (rad) obtained from the International Earth Rotation Service (IERS).

The gravitational acceleration is normalized to a nominal pressure, taking into account a barometric factor f_B = 0.30 × 10^{-8} m·s^{-2}·mbar^{-1}, as recommended by the IAG 1983 resolution n.9.

Instrumental corrections are also applied: (i) the laser beam verticality, (ii) the laser beam divergence and (iii) the overall drift.

The *g* value associated to every measurement session is calculated as the average of *n* measurements and it is referred to a specific height from the floor. The measurement expanded uncertainty is evaluated according to the method of combination of uncertainties as suggested by the ISO GUM guide /5/.

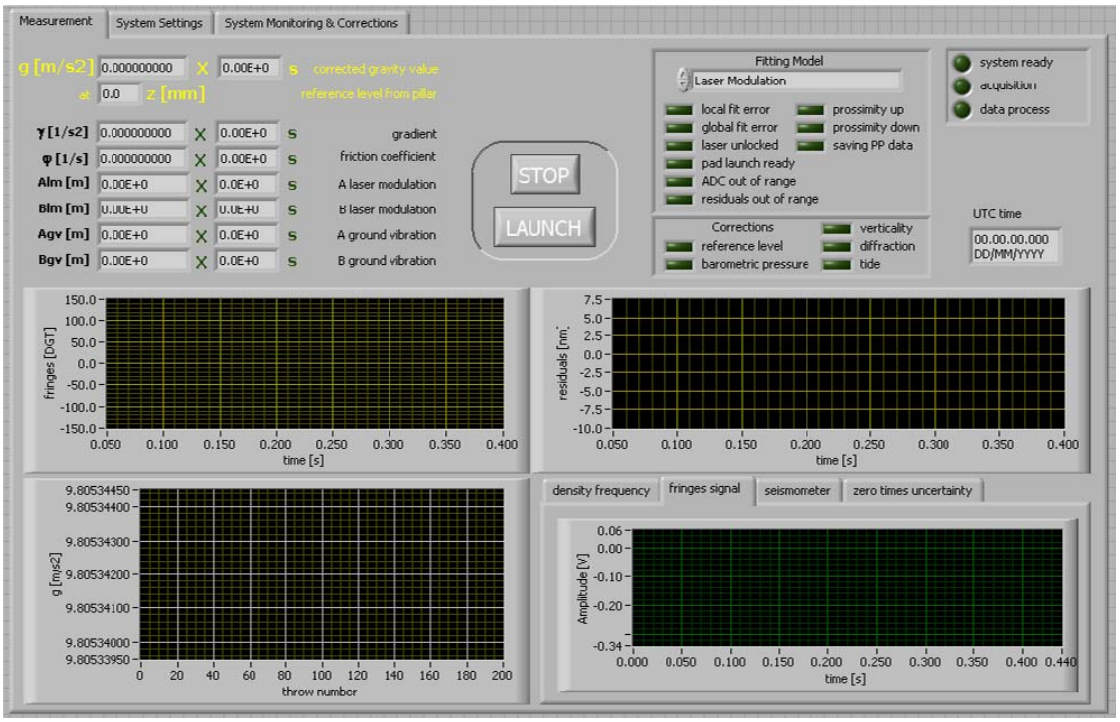

Figure 2.2. GravisoftM - manager front panel

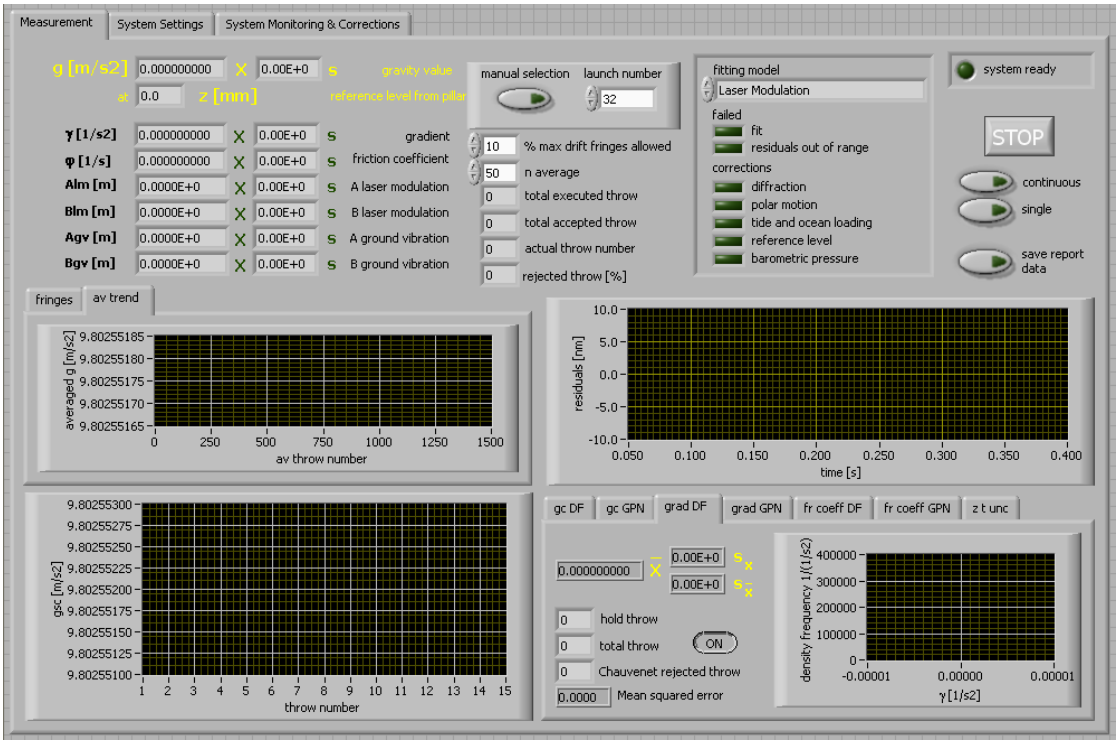

Figure 2.3. GravisoftPP - post-processing front panel

3 MEASUREMENT UNCERTAINTY

The uncertainty associated to the *g* measurement is evaluated by combining the contributions of uncertainty of the IMGC-02 absolute gravimeter, called the instrumental uncertainties to the contribution of uncertainty depending on the observation site.

Uncertainty tables, related to each observation site, are attached to the experimental results below described.

3.1 Instrumental uncertainty of the IMGC-02 absolute gravimeter

Influence factors which are characteristic of the instrument are: vacuum level, non-uniform magnetic field, temperature gradient, electrostatic attraction, mass distribution, laser beam verticality and divergence, overall drift, air gap modulation, length and time standards, retro-reflector balancing, radiation pressure and reference height. A detailed description of these phenomena concerning the present IMGC-02 absolute gravimeter can be found in /1/.

Tab. 3.1 reports the quantitative assessment of the effect of every disturbing factor. The expanded uncertainty at the 95% confidence level (coverage factor k = 2.10 and 19 degrees of freedom) is estimated to be $U = 8.0 \times 10^{-8}$ m·s^{-2}.

3.2 Influence factors characteristic of the observation site

The measurement uncertainty results from the combination of the instrument uncertainty with influence factors that are dependent from the observation site: Coriolis force, floor recoil and geophysical effects, such as local barometric pressure, gravity tides, ocean loading and polar motion.

A detailed description of these phenomena concerning the present IMGC-02 absolute gravimeter can also be found in /1/ and are summarised in the following sub-chapter.

3.2.1 Coriolis force

An object which is moving relative to the earth with a velocity $\vec{v}$, is subjected to the Coriolis acceleration $-2\vec{\omega}_E \times \vec{v}$, due to the earth's angular rotational velocity $\vec{\omega}_E$ (7.3×10^{-5} rad·s^{-1}). A freely falling body with a velocity vector v_{E-W} in the East-West direction is therefore subjected to a Coriolis acceleration with a vertical component a_c which points in the up direction if the vector points in the East direction, towards down direction if the vector points in the West direction. It follows that the test-body experiences the vertical component of the Coriolis acceleration, according to:

$$a_c = 2\omega_E \cdot v_{E-W} \sin(90 - \varphi)$$

where φ is the latitude of the observation site.

An estimation of this effect for each site (latitude) is done and included in the uncertainty table.

Table 3.1. Instrumental uncertainty of the IMGC-02 absolute gravimeter

Influence parameters, x_i	Value	Unit	u_i or a_i	Type A, s_i	Type B, a_i	Correction Δg	Type of distribution	Equivalent variance	Sensitivity coefficients	Contribution to the variance	Degrees of freedom, ν_i	Equivalent standard uncertainty
Drag effect			negligible									
Outgassing effect			negligible									
Non-uniform magnetic field effect			negligible									
Temperature gradient effect		$m \cdot s^{-2}$	±1.5E-09		1.5E-09		U	1.1E-18	1.0E+00	1.1E-18	10	1.1E-09
Effect for Electrostatic			negligible									
Mass distribution effect		$m \cdot s^{-2}$	±5.0E-09		5.0E-09		rectangular	8.3E-18	1.0E+00	8.3E-18	10	2.9E-09
Laser beam verticality correction	6.6E-09	$m \cdot s^{-2}$	±2.1E-09		2.1E-09	6.6E-09	rectangular	1.5E-18	1.0E+00	1.5E-18	15	1.2E-09
Air gap modulation effect			negligible									
Laser effect		$m \cdot s^{-2}$	1.0E-09	1.0E-09				1.0E-18	1.0E+00	1.0E-18	30	1.0E-09
Index of refraction effect			negligible									
Beam divergence correction	1.04E-07	$m \cdot s^{-2}$	1.0E-08	1.0E-08		1.04E-07		1.1E-16	1.0E+00	1.1E-16	10	1.0E-08
Beam share effect	unknown		unknown									
Clock effect		$m \cdot s^{-2}$	6.0E-09	6.0E-09			rectangular	3.6E-17	1.0E+00	3.6E-17	30	6.0E-09
Finges timing effect			negligible									
Finite value of speed of light effect			negligible									
Retroreflector balancing	0.0E+00	m	±1.0E-04		1.0E-04		rectangular	3.3E-09	6.3E-04	1.3E-15	15	3.6E-08
Radiation Pressure effect			negligible									
Reference height	5.0E-01	m	±5.0E-04		5.0E-04		rectangular	8.3E-08	3.0E-06	7.5E-19	30	8.7E-10
					Corr.	**1.11E-07**	**$m \cdot s^{-2}$**	**Variance**		**1.5E-15**	**$m^2 \cdot s^{-4}$**	
					Combined standard uncertainty, u					**3.8E-08**	**$m \cdot s^{-2}$**	
					Degrees of freedom, ν_{eff} (Welch-Satterthwaite formula)					**19**		
					Confidence level, p					**95%**		
					Coverage factor, k (calculated with t-Student)					**2.10**		
					Expanded uncertainty, $U = ku$					**8.0E-08**	**$m \cdot s^{-2}$**	
					Relative expanded uncertainty, $U_{rel} = U/g$					**8.2E-09**		

3.2.2 Floor recoil

The inertial mass of the seismometer is used as a reference point during the trajectory tracking. The natural oscillations due to the ground motion are smoothed and damped according to the seismometer transfer function. From a theoretical point of view, supposing that the ground vibrations are random and uncorrelated with the launch of the test-body, the bias of the average *g* value should tend to zero. Only the data scattering should be affected by the ground vibrations. Experimental tests carried out at INRIM laboratory confirmed that the recoil effect is considered negligible.

Another issue linked to the floor recoil are tilts and translations of the interferometer base. The IMGC-02 interferometer design is insensitive to translations and rotations of the optical block containing the beam splitter and pick-off mirrors. The relevant effect is assessed to be negligible.

3.2.3 Geophysical effects

The measured gravity values are also affected by geophysical effects, such as gravity tide, ocean loading, gravity attraction and loading due to atmospheric pressure variation and change in the centrifugal acceleration due to polar motion. The raw gravity records contain these environmental signals in addition to the experimental noise. The assessment of this noise can be performed only after removing the geophysical effects. Although the theoretical background is beyond the aim of this work, hereafter the information concerning the calculations of the corrections is reported.

3.2.3.1 Local barometric pressure

Local air pressure variations affect absolute gravity measurements. A portion of the total mass attraction of the earth is due to atmosphere. As the pressure at the surface increases, the integrated mass above the observation point also increases due to the average density. It follows an upward force which decreases the local gravity value. Another consequence of higher pressure is an increased load on the surface which causes a depression in the crust. As a consequence the *g* value increases. Between the two competing effects, the strong one is the mass attraction which is about 12 times larger than the depression in the crust. A local barometric pressure increasing makes the gravity value decreasing. As recommended by the IAG 1983 resolution n.9, the barometric factor is defined as f_B = 0.30 μGal·mbar^{-1}.

Moreover, the measured gravity is referred to a nominal pressure P_n by applying the following correction:

$$\Delta g_{pr} = f_B \cdot (P_o - P_n)$$

where P_o is the observed atmospheric pressure.

The nominal pressure at the site is defined as:

$$P_n = 1013.25 \cdot \left(1 - 0.0065 \frac{h_m}{288.15}\right)^{5.2559}$$

where P_n is introduced in mbar and h_m, the topographic elevation, in m.

The barometer adopted is the Druck DPI 280. The calibration of this device, performed on the range 800-1100 mbar showed a fractional accuracy of 1×10^{-4}. If frequent calibration is performed, the residual uncertainty assigned after the correction is therefore negligible (0.03 μGal).

3.2.3.2 Gravity tide and ocean loading

Gravity tide includes the body earth tide and attraction-loading effects from ocean tide. In particular the first one is mainly due to the external influence of the sun and moon. The latter one is a consequence of the first, because the effect of luni-solar tide is a variation of the height of the oceans twice daily. The redistribution of the ocean's surface affects the value of gravity measured at a particular site. It has to be underlined that the effect is stronger and not perfectly known at seaside, especially in an observation site with a high altitude.

The gravity tide corrections can be computed either through calculation based on models or by fitting gravimetric measured data, normally acquired by means of relative gravimeters. To generate the tide corrections, the IMGC-02 is currently using subroutines based on the ETGTAB software written by late Prof. H.-G Wenzel, Geodetic Institute, Karlsruhe University. This program computes body tidal parameters and generates time series of body tides starting from the geographic coordinates of the observation point. The tidal parameters are amplitude and phase of defined waves. Parameters of the ocean loading are calculated with the FES2004 model computed by OLMPP (Scherneck) Onsala Space Observatory (http://www.oso.chalmers.se/~loading/).

In literature it is reported that mean typical uncertainties after correction are respectively 0.3 μGal and 0.2 μGal for body earth tide and ocean loading.

3.2.3.3 Polar motion

The rotation of the earth around its pole generates a centrifugal force which deforms the earth into an ellipsoid. Any changes in the rotation rate or the location of the rotation pole affect the amplitude and the direction of the centrifugal force.

The gravitational acceleration comprises the centrifugal force, therefore the above mentioned changes directly affects the measured *g* value. The surface of the earth is also deformed by variations in the centrifugal force. It follows that also the earth's potential energy and the position of the observation point respect to the centre if the earth changes. Wahr discussed this subject and suggested the so called polar motion correction:

$$\Delta g_{pm} = -1.164 \cdot \omega_E^2 \cdot a \cdot 2 \cdot \sin\varphi \cdot \cos\varphi \cdot \left(x \cos\lambda - y \sin\lambda\right)$$

The correction is given in $m \cdot s^{-2}$. ω_E is the earth's angular rotational velocity, a = 6378136 m is the equatorial radius (semi-major axis) of the reference ellipsoid, φ and λ are respectively the geodetic latitude and longitude of the observation station. The daily pole coordinates x and y are obtained from the International Earth Rotation Service (IERS) at the web-site: http://hpiers.obspm.fr/eop-pc/.

The uncertainty of polar motion, after the correction, is considered negligible.

3.2.4 Scattering of measurements

This effect is estimated with the experimental standard deviation of the mean *g* value. It is strongly depended on the ground vibrations and floor recoil.

4 EXPERIMENTAL RESULTS

The measurements was carried out by the INRIM team with the extremely friendly and useful support of the INGV-Catania Section team (fig. 4).

Figure 4. Pictures of the INGV and INRIM team

4.1 Catania - INGV

The observation station of Catania - INGV is located at the Gravity Laboratory of the Istituto Nazionale di Geofisica e Vulcanologia INGV, fig. 4.1.1 and 4.1.2.

The measurement was carried on 08-09 July 2009.

The position of the measurement point (fig. 4.1.3) referred to the room is showed on the plan of the building, fig. 4.1.4. The orientation of the instrument is showed by the red triangle where the black square represents the laser body.

The instrument processed and stored 1337 trajectories.

The measured data are filtered by applying rejecting criteria. The most critical factor is the visibility variation of the interference signal during the trajectory, which highlights an horizontal motion of the test-body. The effect due to the Coriolis force and the beam share are minimized by rejecting those launches with a decrease of visibility bigger that 10%.

Outliers are found by applying the Chauvenet criterion to the estimating parameters such as the vertical gradient, the friction of residual air and to the estimated *g* value.

The final *g* value is obtained by averaging 477 trajectories. Table 4.1.1. reports the most important experimental results. Other information concerning the apparatus setup are reported in table 4.1.2.

The time series of the post-processed trajectories, data sets (each correspondent to the average of 50 launches) and trajectory residuals are reported in figure 4.1.5. The apparatus experienced an oscillation of about $\pm 15.0 \times 10^{-8}$ m·s^{-2}. The averaged trajectory residuals after the measurement session are within $\pm 1 \times 10^{-9}$ m.

The graphs reported in figure 4.1.6. represent the density frequency histograms and normal probability graphs of the *g* value, gradient and friction coefficient of the measurement session. The χ^2 test rejects the null hypothesis, i.e. the normal distribution, with a 20% risk error.
Figure 4.1.7. reports ambient temperature, local barometric pressure and launch chamber pressure acquired at each launch and the applied tide corrections.

The measurement uncertainty is summarized in table 4.1.3. It includes the instrumental uncertainty reported in tab. 3.1.

Figure 4.1.1. Observation site in Catania - INGV

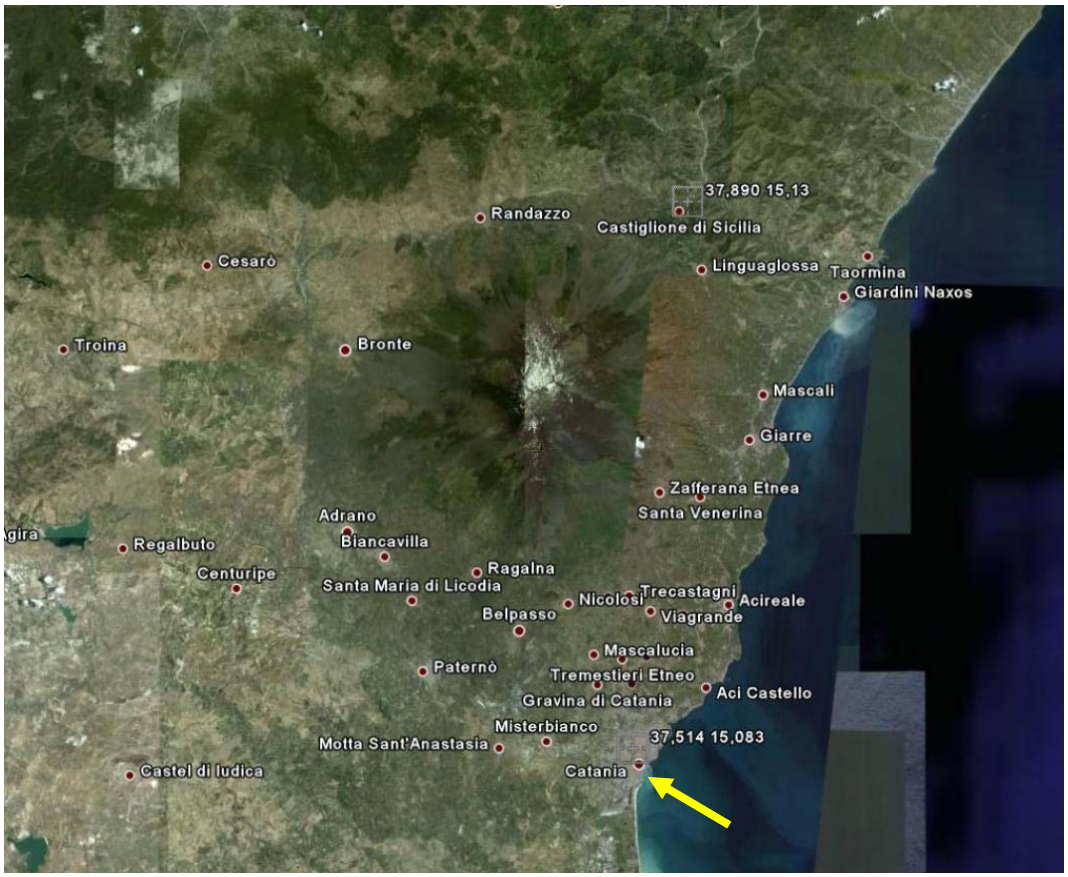

Figure 4.1.2. Satellite image of the observation site in Catania - INGV

Figure 4.1.3. Observation station in Catania - INGV

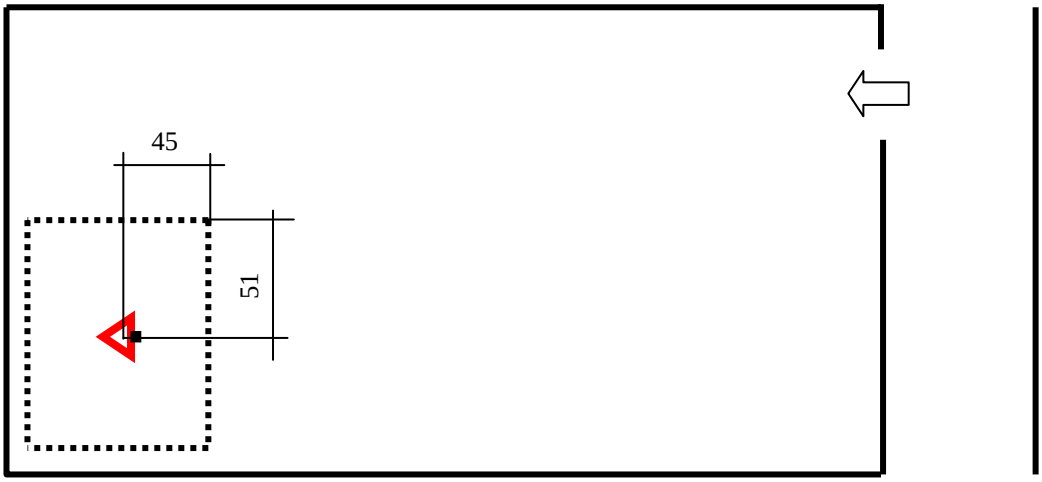

Figure 4.1.4. Plane of the building in Catania - INGV

Table 4.1.1. Experimental results in Catania – INGV – Gravity Lab

Observation Station: **Catania – INGV – Gravity Lab**	
Observation start (data and time in UTC)	2009/07/08 13:15:38
Observation stop (data and time in UTC)	2009/07/09 06:51:24
Geodetic longitude	λ = 15.083°
Geodetic latitude	φ = 37.514°
Topographic elevation	H_T = 50 m
Nominal pressure at the observation site	P_N = 1007.3 mbar
Pole coordinates in IERS system	x = 0.157233", y = 0.526775"
Measurement parameters	
Total observation time	T_m = 17.60 h
Measurement rate	m_r = 100 h^{-1}
Total processed and stored throws	n_{ps} = 1337
Temperature range	T = (30.2 ÷ 32.0)°C
Local barometric pressure (mean)	P = 1009.2 mbar
χ^2 test (80% confidence level)	χ^2_{max} = 30.8; χ^2_{min} = 14.0; χ^2_{exp} = 39.7
Corrections	
Laser beam verticality	Δg_{bv} = +0.6 × 10^{-8} m·s^{-2}
Laser beam divergence	Δg_{bd} = +10.9 × 10^{-8} m·s^{-2}
Overall drift	Δg_d = -2.4 × 10^{-8} m·s^{-2}
Polar motion	Δg_{pm} = -0.3 × 10^{-8} m·s^{-2}
Tide and ocean loading (mean)	Δg_{tol} = -33.2 × 10^{-8} m·s^{-2}
Local barometric pressure (mean)	Δg_{bp} = +0.8 × 10^{-8} m·s^{-2}
Results	
corrected mean *g* value	**g_{mv} = 980 031 505.9 × 10^{-8} m·s^{-2}**
Reference height	**h_{ref} = 500.9 mm**
Number of throws accepted for the average	**n = 477**
Experimental standard deviation	s_g = 65.5 × 10^{-8} m·s^{-2}
Experimental standard deviation of the mean value	**s_{gm} = 3.0 × 10^{-8} m·s^{-2}**
Measurement combined uncertainty	u_{gm} = 5.2 × 10^{-8} m·s^{-2}
Measurement expanded uncertainty (p = 95%, ν = 59, k = 2.00)	**U_{gm} = 10.4 × 10^{-8} m·s^{-2}**
Vertical gradient	γ = (278.6 ± 15.7) × 10^{-8} s^{-2}

Table 4.1.2. Apparatus setup in Catania – INGV – Gravity Lab

Instrument orientation	See fig. 4.1.4.
Fitting Model	Laser mod.
Fringe visibility threshold	f_{vt} = 10%
Measurements each set	n_{ma} = 50
Waveform digitizer sampling frequency	S_f = 50 MHz
Laser wavelength	λ_l = 632.9912130 × 10^{-9} m
Clock frequency	f_c = 10000000.0075 Hz
Vertical gradient input	γ = 0.000002700 s^{-2}
Rise station number	n_{rs} = 350
Leaved upper stations	n_{sl} = 2
Laser modulation frequency	f_{lm} = 1165.2 Hz

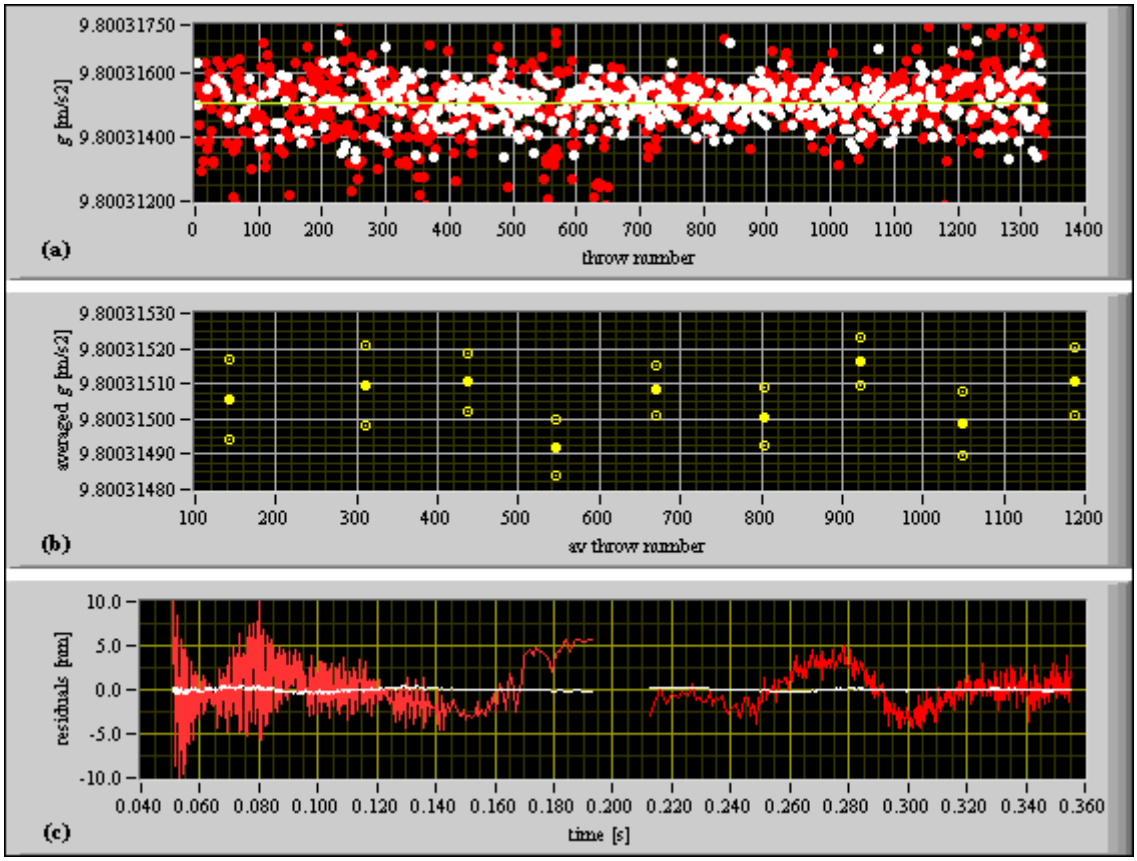

Figure 4.1.5. Time series (rejected-red, accepted-white) (a), Data sets (average of 50 launches) (b), trajectory residuals (one launch-red, average-white) (c) in Catania - INGV

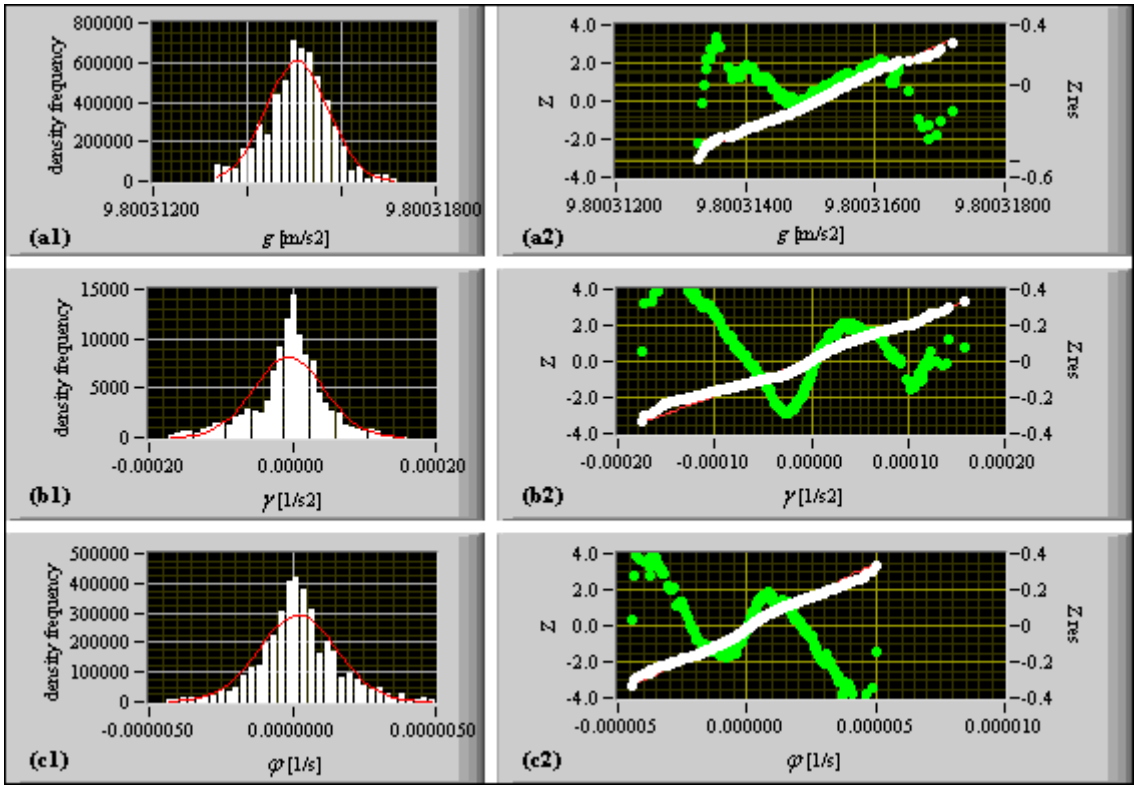

Figure 4.1.6. Density frequency graphs (1) and normal probability graphs (2) of the *g* value (a), gradient (b) and friction coefficient (c) measured in Catania - INGV

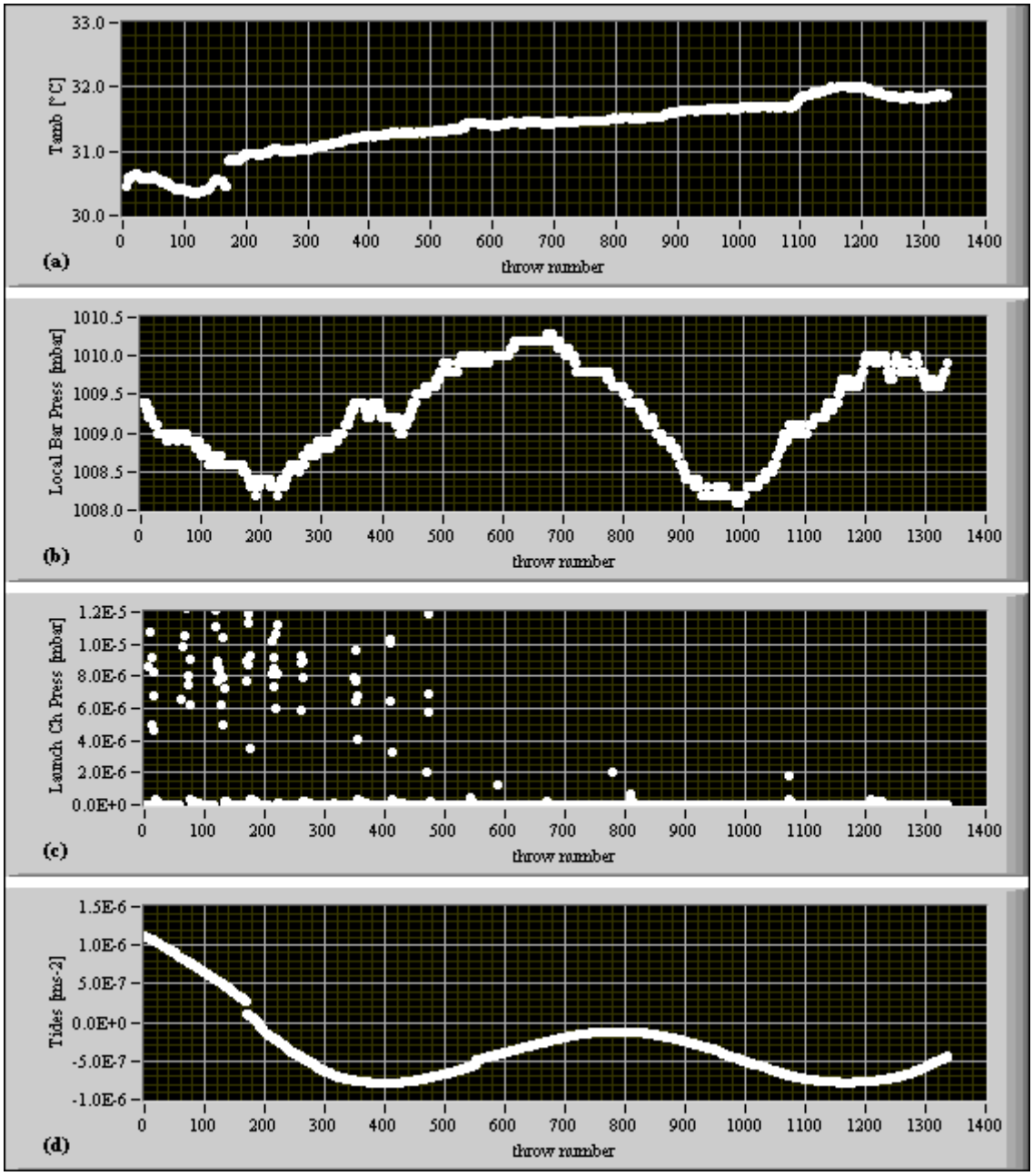

Figure 4.1.7. Ambient temp. (a), local barometric pressure (b) and launch chamber pressure (c) acquired at each launch and applied tide corrections (d) in Catania - INGV

Remarks

During the measurement session the overall drift was -2.4×10^{-8} ms^{-2}. The trajectory was reconstructed with the model that takes into account the laser modulation. The best results were obtained by removing the 2 upper stations from the fit. The average of the trajectory residuals shows that the floor is really stiff and the scattering of the data highlights that the observation site is quite.

The measurements of the free-fall acceleration are considered to be correct within the evaluated uncertainty.

There is a huge difference (tens of microgals) between the results obtained in 2009 and those obtained in 2008 (see Technical Report INRIM n.141 September 2008). Moreover, the results obtained in 2009 are compatible with those obtained in 2007 (see Technical Report INRIM n.73 November 2007). The reason for these strong differences is under analysis.

Table 4.1.3. Measurement uncertainty in Catania - INGV

Influence parameters, x_i	Value	Unit	u_i or a_i	Type A, s_i	Type B, a_i	Correction Δg	Type of distribution	Equivalent variance	Sensitivity coefficients	Contribution to the variance	Degrees of freedom, ν_i	Equivalent standard uncertainty
Instrument uncertainty		$m \cdot s^{-2}$	3.8E-08	3.8E-08				1.5E-15	1.00E+00	1.5E-15	19	3.8E-08
Coriolis effect		$m \cdot s^{-2}$	2.9E-08		2.9E-08		rectangular	2.8E-16	1.00E+00	2.8E-16	10	1.7E-08
Floor recoil effect			negligible									
Barometric pressure correction	8.0E-09	$m \cdot s^{-2}$	1.0E-08		1.0E-08	8.0E-09	rectangular	3.3E-17	1.00E+00	3.3E-17	15	5.8E-09
Tide correction	-3.3E-07	$m \cdot s^{-2}$	3.0E-09	3.0E-09		-3.3E-07		9.0E-18	1.00E+00	9.0E-18	15	3.0E-09
Ocean loading correction		$m \cdot s^{-2}$	2.0E-09	2.0E-09				4.0E-18	1.00E+00	4.0E-18	15	2.0E-09
Polar motion correction	-3.0E-09	$m \cdot s^{-3}$	negligible			-3.0E-09						
Standard deviation of the mean value		$m \cdot s^{-2}$	3.0E-08	3.0E-08				9.0E-16	1.00E+00	9.0E-16	476	3.0E-08
					Corr.	**-3.3E-07**	**$m \cdot s^{-2}$**	**Variance**		**2.7E-15**	**$m^2 \cdot s^{-4}$**	
					Combined standard uncertainty, u					**5.2E-08**	**$m \cdot s^{-2}$**	
					Degrees of freedom, ν_{eff} (Welch-Satterthwaite formula)					**59**		
					Confidence level, p					**95%**		
					Coverage factor, k (calculated with t-Student)					**2.00**		
					Expanded uncertainty, $U = ku$					**1.0E-07**	**$m \cdot s^{-2}$**	
					Relative expanded uncertainty, $U_{rel} = U/g$					**1.1E-08**		

4.2 Serra La Nave

The observation station of Serra La Nave is located at the Osservatorio Astrofisico di Catania "Mario G. Fracastoro", fig. 4.2.1 and 4.2.2.

The measurement was carried on 09-10 July 2009.

The position of the measurement point (fig. 4.2.3) referred to the room is showed on the plan of the building, fig. 4.2.4. The orientation of the instrument is showed by the red triangle where the black square represents the laser body.

The instrument processed and stored 1462 trajectories.

The measured data are filtered by applying rejecting criteria. The most critical factor is the visibility variation of the interference signal during the trajectory, which highlights an horizontal motion of the test-body. The effect due to the Coriolis force and the beam share are minimized by rejecting those launches with a decrease of visibility bigger that 10%.

Outliers are found by applying the Chauvenet criterion to the estimating parameters such as the vertical gradient, the friction of residual air and to the estimated *g* value.

The final *g* value is obtained by averaging 372 trajectories. Table 4.2.1. reports the most important experimental results. Other information concerning the apparatus setup are reported in table 4.2.2.

The time series of the post-processed trajectories, data sets (each correspondent to the average of 50 launches) and trajectory residuals are reported in figure 4.2.5. The apparatus experienced an oscillation of about $\pm 10.0 \times 10^{-8}$ m·s^{-2}. The averaged trajectory residuals after the measurement session are within $\pm 1 \times 10^{-9}$ m.

The graphs reported in figure 4.2.6. represent the density frequency histograms and normal probability graphs of the *g* value, gradient and friction coefficient of the measurement session. The χ^2 test rejects the null hypothesis, i.e. the normal distribution, with a 20% risk error.
Figure 4.2.7. reports ambient temperature, local barometric pressure and launch chamber pressure acquired at each launch and the applied tide corrections.

The measurement uncertainty is summarized in table 4.2.3. It includes the instrumental uncertainty reported in tab. 3.1.

Figure 4.2.1. Observation site at Serra La Nave

Figure 4.2.2. Satellite image of the observation site at Serra La Nave

Figure 4.2.3. Observation station at Serra La Nave

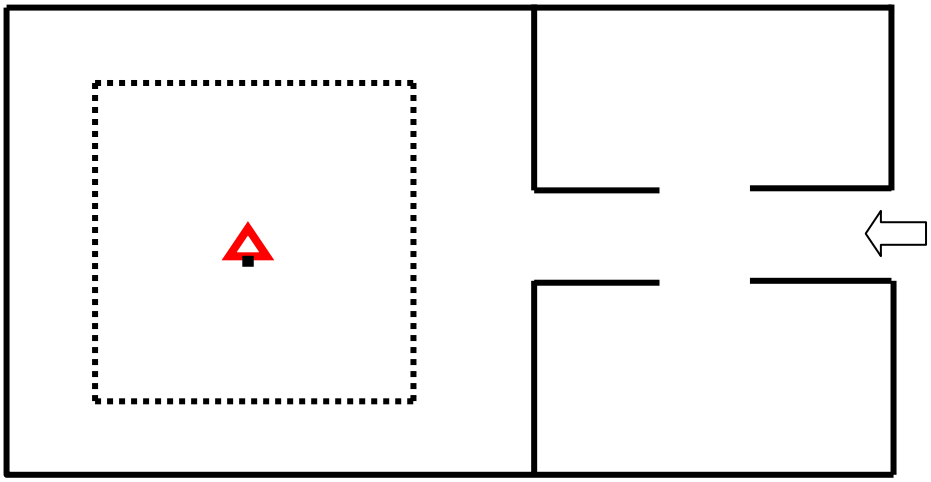

Figure 4.2.4. Plane of the building at Serra La Nave

Table 4.2.1. Experimental results at Serra La Nave

Observation Station: **Serra La Nave**	
Observation start (data and time in UTC)	2009/07/09 15:12:18
Observation stop (data and time in UTC)	2009/07/10 08:28:27
Geodetic longitude	λ = 14.973°
Geodetic latitude	φ = 37.694°
Topographic elevation	H_T = 1730 m
Nominal pressure at the observation site	P_N = 822.0 mbar
Pole coordinates in IERS system	x = 0.159873", y = 0.525814"
Measurement parameters	
Total observation time	T_m = 17.27 h
Measurement rate	m_r = 95 h^{-1}
Total processed and stored throws	n_{ps} = 1462
Temperature range	T = (38.0 ÷ 40.3)°C
Local barometric pressure (mean)	P = 830.6 mbar
χ^2 test (80% confidence level)	χ^2_{max} = 28.4; χ^2_{min} = 12.4; χ^2_{exp} = 30.6
Corrections	
Laser beam verticality	Δg_{bv} = +0.6 × 10^{-8} m·s^{-2}
Laser beam divergence	Δg_{bd} = +10.9 × 10^{-8} m·s^{-2}
Overall drift	Δg_d = -20.6 × 10^{-8} m·s^{-2}
Polar motion	Δg_{pm} = -0.3 × 10^{-8} m·s^{-2}
Tide and ocean loading (mean)	Δg_{tol} = -39.1 × 10^{-8} m·s^{-2}
Local barometric pressure (mean)	Δg_{bp} = +2.6 × 10^{-8} m·s^{-2}
Results	
corrected mean *g* value	**g_{mv} = 979 641 630.8 × 10^{-8} m·s^{-2}**
Reference height	**h_{ref} = 498.2 mm**
Number of throws accepted for the average	**n = 372**
Experimental standard deviation	s_g = 42.7 × 10^{-8} m·s^{-2}
Experimental standard deviation of the mean value	**s_{gm} = 2.2 × 10^{-8} m·s^{-2}**
Measurement combined uncertainty	u_{gm} = 4.7 × 10^{-8} m·s^{-2}
Measurement expanded uncertainty (p = 95%, ν = 42, k = 2.02)	**U_{gm} = 9.6 × 10^{-8} m·s^{-2}**
Vertical gradient	γ = (335.1 ± 10.6) × 10^{-8} s^{-2}

Table 4.1.2. Apparatus setup at Serra La Nave

Instrument orientation	See fig. 4.2.4.
Fitting Model	Laser mod.
Fringe visibility threshold	f_{vt} = 10%
Measurements each set	n_{ma} = 50
Waveform digitizer sampling frequency	S_f = 50 MHz
Laser wavelength	λ_l = 632.9912130 × 10^{-9} m
Clock frequency	f_c = 10000000.0075 Hz
Vertical gradient input	γ = 0.000002700 s^{-2}
Rise station number	n_{rs} = 350
Leaved upper stations	n_{sl} = 2
Laser modulation frequency	f_{lm} = 1165.2 Hz

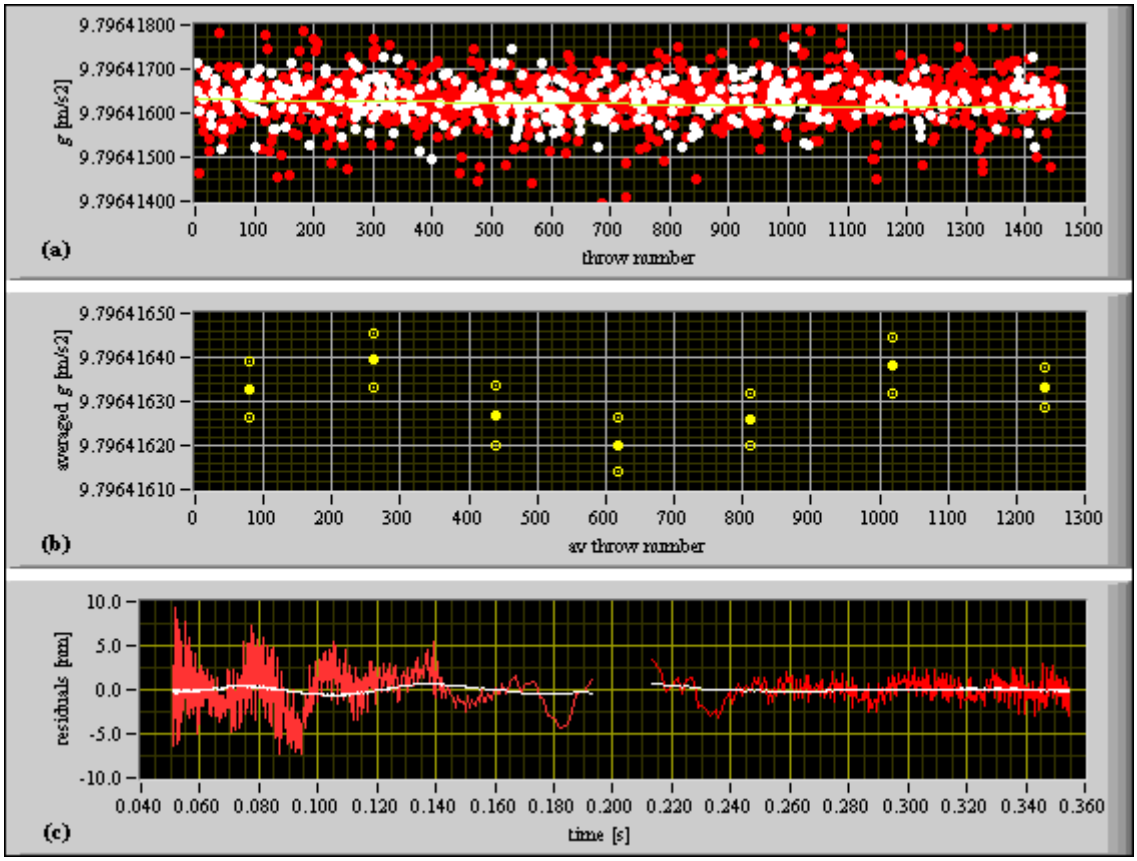

Figure 4.2.5. Time series (rejected-red, accepted-white) (a), Data sets (average of 50 launches) (b), trajectory residuals (one launch-red, average-white) (c) at Serra La Nave

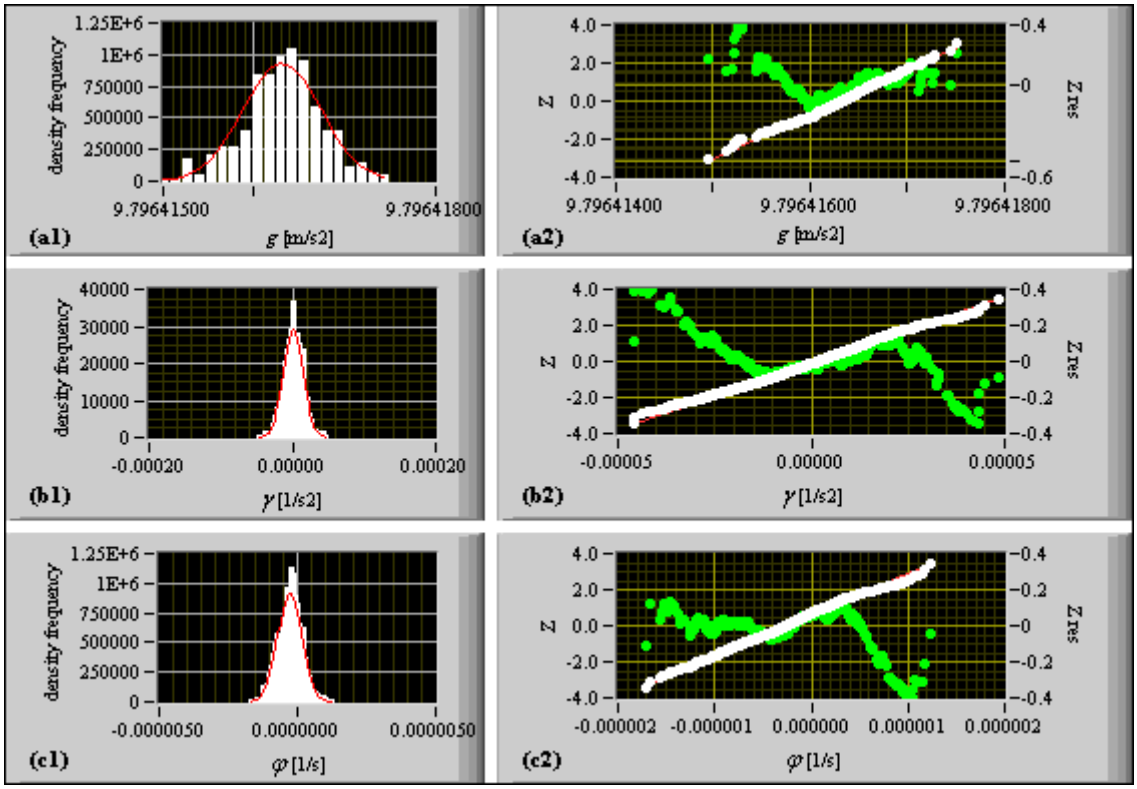

Figure 4.2.6. Density frequency graphs (1) and normal probability graphs (2) of the *g* value (a), gradient (b) and friction coefficient (c) measured at Serra La Nave

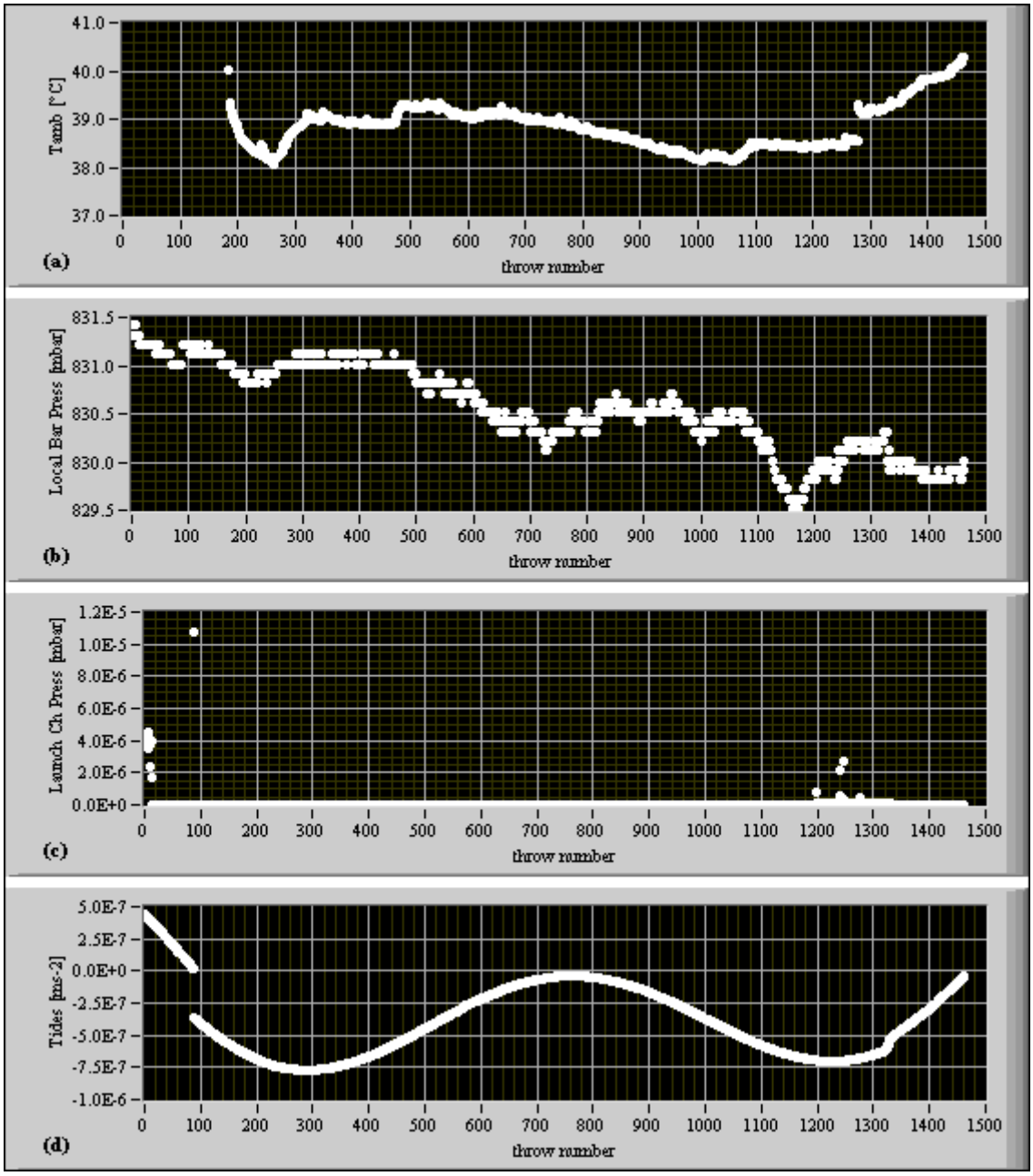

Figure 4.2.7. Ambient temp. (a), local barometric pressure (b) and launch chamber pressure (c) acquired at each launch and applied tide corrections (d) at Serra La Nave

Remarks

During the measurement session the overall drift was -20.6 $\times 10^{-8}$ ms^{-2}. The trajectory was reconstructed with the model that takes into account the laser modulation. The best results were obtained by removing the 2 upper stations from the fit. The average of the trajectory residuals shows that the floor is really stiff and the scattering of the data highlights that the observation site is quite.

The measurements of the free-fall acceleration are considered to be correct within the evaluated uncertainty.

Table 4.2.3. Measurement uncertainty at Serra La Nave

Influence parameters, x_i	Value	Unit	u_i or a_i	Type A, s_i	Type B, a_i	Correction Δg	Type of distribution	Equivalent variance	Sensitivity coefficients	Contribution to the variance	Degrees of freedom, ν_i	Equivalent standard uncertainty
Instrument uncertainty		$m \cdot s^{-2}$	3.8E-08	3.8E-08				1.5E-15	1.00E+00	1.5E-15	19	3.8E-08
Coriolis effect		$m \cdot s^{-2}$	2.9E-08		2.9E-08		rectangular	2.8E-16	1.00E+00	2.8E-16	10	1.7E-08
Floor recoil effect			negligible									
Barometric pressure correction	2.6E-08	$m \cdot s^{-2}$	1.0E-08		1.0E-08	2.6E-08	rectangular	3.3E-17	1.00E+00	3.3E-17	15	5.8E-09
Tide correction	-3.9E-07	$m \cdot s^{-2}$	3.0E-09	3.0E-09		-3.9E-07		9.0E-18	1.00E+00	9.0E-18	15	3.0E-09
Ocean loading correction		$m \cdot s^{-2}$	2.0E-09	2.0E-09				4.0E-18	1.00E+00	4.0E-18	15	2.0E-09
Polar motion correction	-3.0E-09	$m \cdot s^{-3}$	negligible			-3.0E-09						
Standard deviation of the mean value		$m \cdot s^{-2}$	2.2E-08	2.2E-08				4.8E-16	1.00E+00	4.8E-16	371	2.2E-08
					Corr.	**-3.7E-07**	**$m \cdot s^{-2}$**	**Variance**		**2.3E-15**	**$m^2 \cdot s^{-4}$**	
					Combined standard uncertainty, u					**4.8E-08**	**$m \cdot s^{-2}$**	
					Degrees of freedom, ν_{eff} (Welch-Satterthwaite formula)					**42**		
					Confidence level, p					**95%**		
					Coverage factor, k (calculated with t-Student)					**2.02**		
					Expanded uncertainty, $U = ku$					**9.6E-08**	**$m \cdot s^{-2}$**	
					Relative expanded uncertainty, $U_{rel} = U/g$					**9.8E-09**		

4.3 Montagnola

The observation station of Montagnola is located in a building of the arrive station of the cabin-lift, fig. 4.3.1 and 4.3.2.

The measurement was carried on 10-11 July 2009.

The position of the measurement point (fig. 4.3.3) referred to the room is showed on the plan of the building, fig. 4.3.4. The orientation of the instrument is showed by the red triangle where the black square represents the laser body.

The instrument processed and stored 1422 trajectories.

The measured data are filtered by applying rejecting criteria. The most critical factor is the visibility variation of the interference signal during the trajectory, which highlights an horizontal motion of the test-body. The effect due to the Coriolis force and the beam share are minimized by rejecting those launches with a decrease of visibility bigger that 10%.

Outliers are found by applying the Chauvenet criterion to the estimating parameters such as the vertical gradient, the friction of residual air and to the estimated *g* value.

The final *g* value is obtained by averaging 496 trajectories. Table 4.3.1. reports the most important experimental results. Other information concerning the apparatus setup are reported in table 4.3.2.

The time series of the post-processed trajectories, data sets (each correspondent to the average of 50 launches) and trajectory residuals are reported in figure 4.3.5. The apparatus experienced an oscillation of about $\pm 10.0 \times 10^{-8}$ m·s^{-2}. The averaged trajectory residuals after the measurement session are within $\pm 4.0 \times 10^{-9}$ m.

The graphs reported in figure 4.3.6. represent the density frequency histograms and normal probability graphs of the *g* value, gradient and friction coefficient of the measurement session. The χ^2 test rejects the null hypothesis, i.e. the normal distribution, with a 20% risk error.
Figure 4.3.7. reports ambient temperature, local barometric pressure and launch chamber pressure acquired at each launch and the applied tide corrections.

The measurement uncertainty is summarized in table 4.3.3. It includes the instrumental uncertainty reported in tab. 3.1.

Figure 4.3.1. Observation site in Montagnola

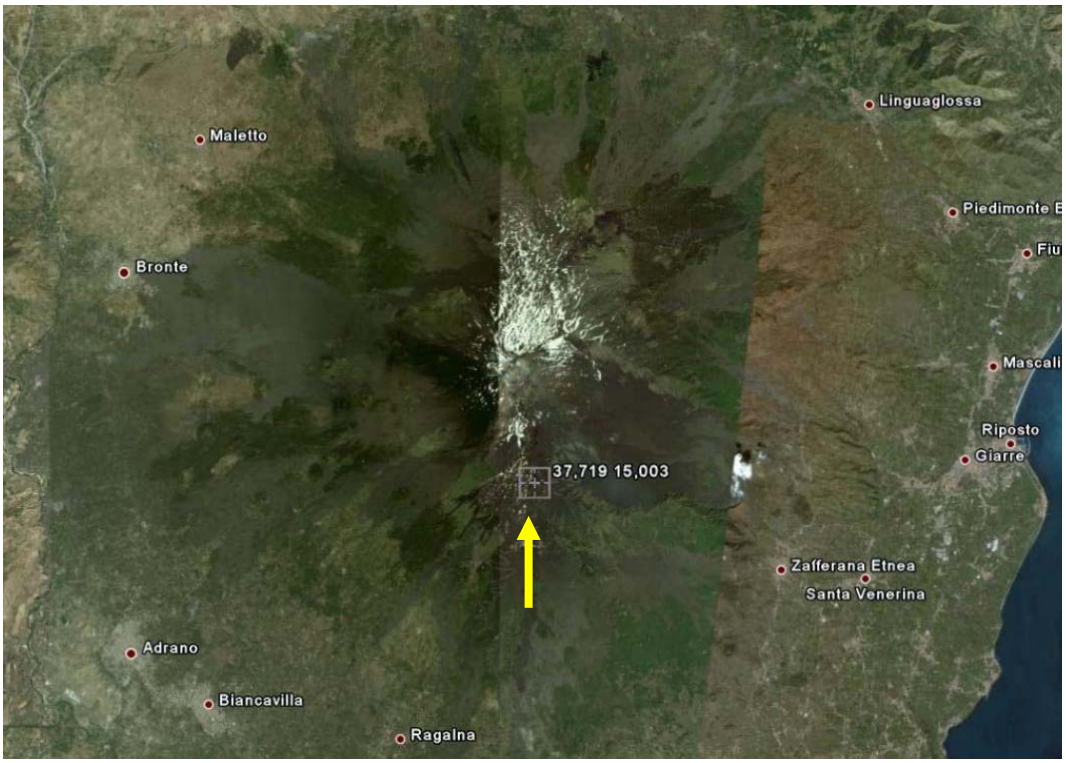

Figure 4.3.2. Satellite image of the observation site in Montagnola

Figure 4.3.3. Observation station in Montagnola

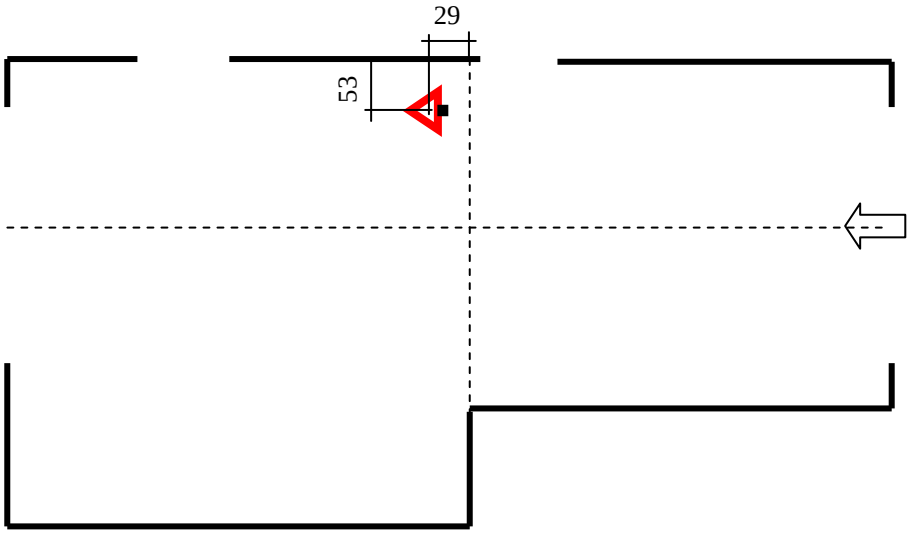

Figure 4.3.4. Plane of the building in Montagnola

Table 4.3.1. Experimental results in Montagnola

Observation Station: **Montagnola**	
Observation start (data and time in UTC)	2009/07/10 17:09:46
Observation stop (data and time in UTC)	2009/07/11 06:19:29
Geodetic longitude	λ = 15.003°
Geodetic latitude	φ = 37.719°
Topographic elevation	H_T = 2550 m
Nominal pressure at the observation site	P_N = 742.1mbar
Pole coordinates in IERS system	x = 0.162761", y = 0.524983"
Measurement parameters	
Total observation time	T_m = 13.16 h
Measurement rate	m_r = 108 h^{-1}
Total processed and stored throws	n_{ps} = 1422
Temperature range	T = (15.3 ÷ 20.8)°C
Local barometric pressure (mean)	P = 756.3 mbar
χ^2 test (80% confidence level)	χ^2_{max} = 32.0; χ^2_{min} = 14.8; χ^2_{exp} = 43.2
Corrections	
Laser beam verticality correction	Δg_{bv} = +0.6 × 10^{-8} m·s^{-2}
Laser beam divergence correction	Δg_{bd} = +10.9 × 10^{-8} m·s^{-2}
Overall drift	Δg_d = -14.9 × 10^{-8} m·s^{-2}
Polar motion correction	Δg_{pm} = -0.4 × 10^{-8} m·s^{-2}
Tide and ocean loading correction (mean)	Δg_{tol} = -35.6 × 10^{-8} m·s^{-2}
Local barometric pressure correction (mean)	Δg_{bp} = +4.3 × 10^{-8} m·s^{-2}
Results	
corrected mean *g* value	**g_{mv} = 979 468 506.4 × 10^{-8} m·s^{-2}**
Reference height	**h_{ref} = 498.1 mm**
Number of throws accepted for the average	**n = 496**
Experimental standard deviation	s_g = 63.6 × 10^{-8} m·s^{-2}
Experimental standard deviation of the mean value	**s_{gm} = 2.8 × 10^{-8} m·s^{-2}**
Measurement combined uncertainty	u_{gm} = 5.0 × 10^{-8} m·s^{-2}
Measurement expanded uncertainty (p = 95%, ν = 54, k = 2.01)	**U_{gm} = 10.0 × 10^{-8} m·s^{-2}**
Vertical gradient	γ = (331.7 ± 16.3) × 10^{-8} s^{-2}

Table 4.3.2. Apparatus setup in Montagnola

Instrument orientation	See fig. 4.3.4.
Fitting Model	Laser mod. & ground vibr. (19.9 Hz)
Fringe visibility threshold	f_{vt} = 10%
Measurements each set	n_{ma} = 50
Waveform digitizer sampling frequency	S_f = 50 MHz
Laser wavelength	λ_l = 632.9912130 × 10^{-9} m
Clock frequency	f_c = 10000000.0075 Hz
Vertical gradient input	γ = 0.000002700 s^{-2}
Rise station number	n_{rs} = 350
Leaved upper stations	n_{sl} = 2
Laser modulation frequency	f_{lm} = 1165.2 Hz

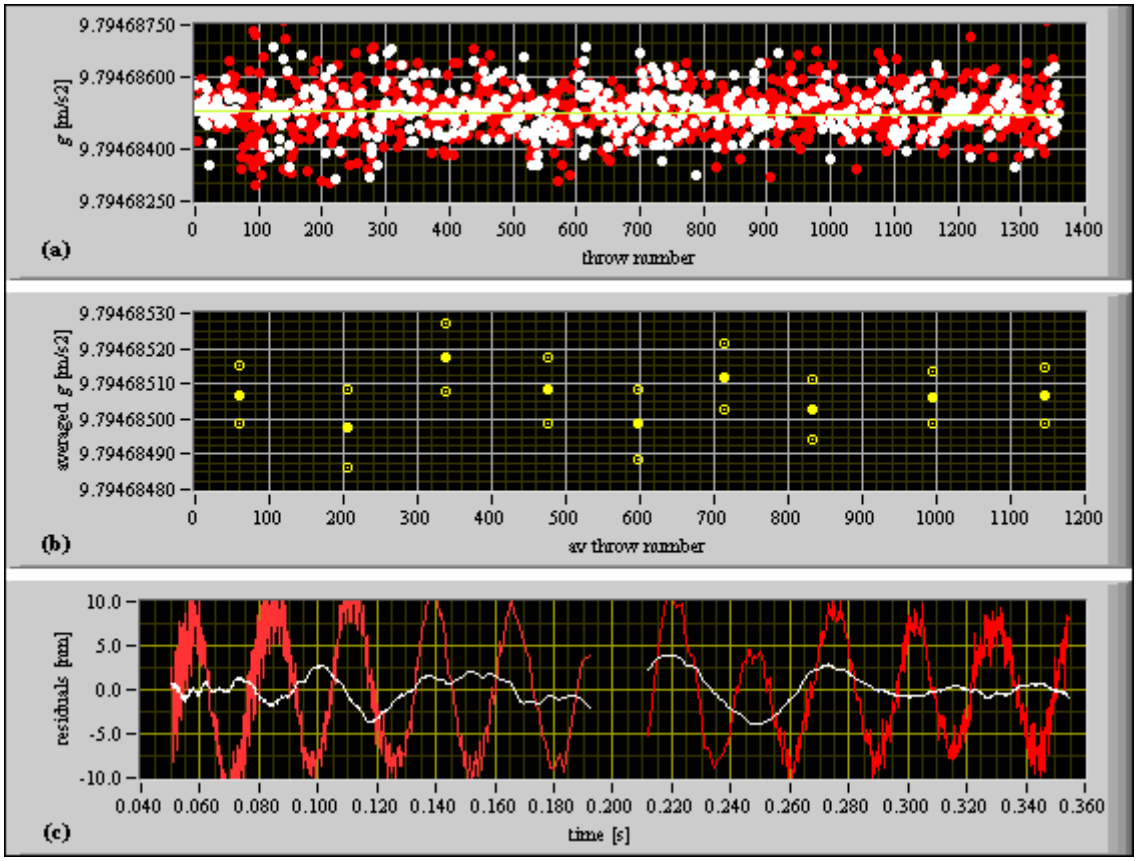

Figure 4.3.5. Time series (rejected-red, accepted-white) (a), Data sets (average of 50 launches) (b), trajectory residuals (one launch-red, average-white) (c) in Montagnola

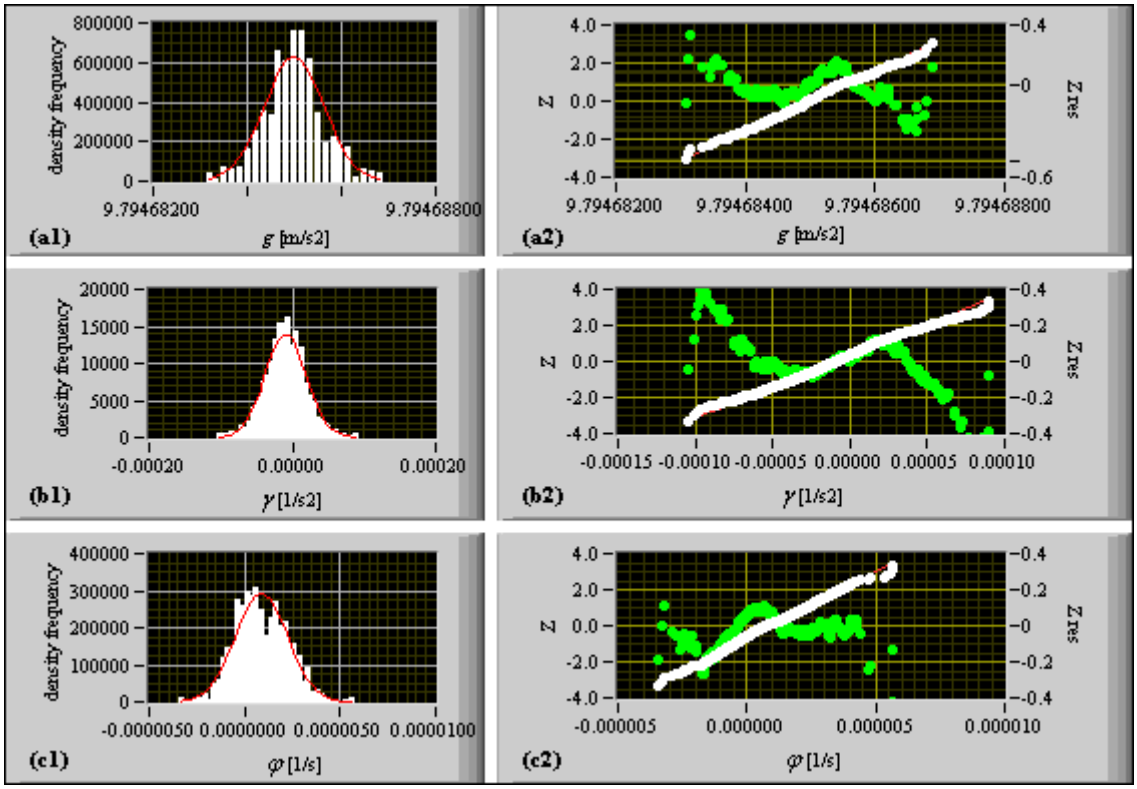

Figure 4.3.6. Density frequency graphs (1) and normal probability graphs (2) of the *g* value (a), gradient (b) and friction coefficient (c) measured in Montagnola

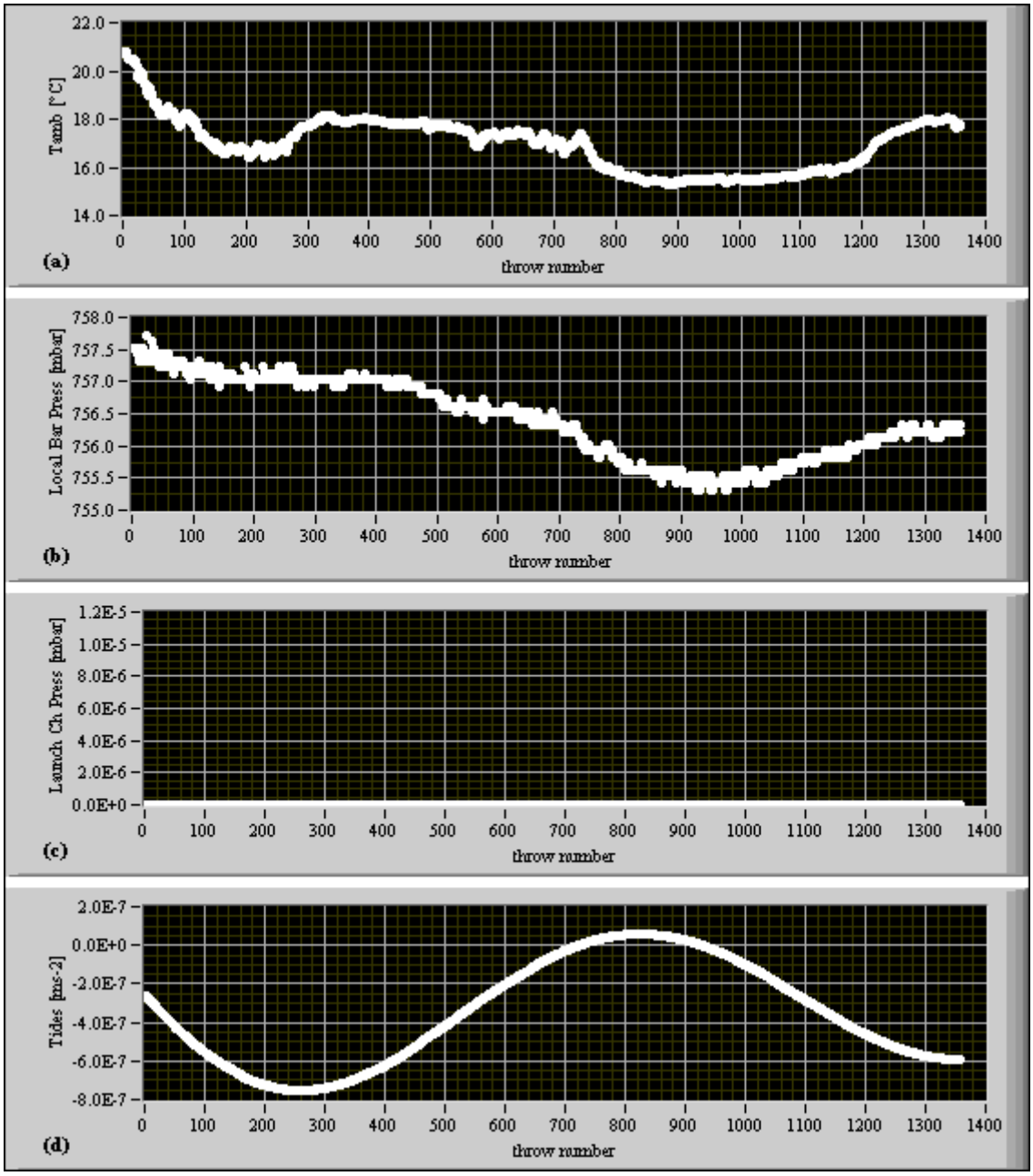

Figure 4.3.7. Ambient temp. (a), local barometric pressure (b) and launch chamber pressure (c) acquired at each launch and applied tide corrections (d) in Montagnola

Remarks

During the measurement session the overall drift was -14.9 $\times 10^{-8}$ ms^{-2}. The trajectory was reconstructed with the model that takes into account the laser modulation and the vibration of the inertial system. The best results were obtained by removing the 2 upper stations from the fit. The average of the trajectory residuals shows that the floor is stiff and the scattering of the data highlights that the observation site is quite.

The measurements of the free-fall acceleration are considered to be correct within the evaluated uncertainty.

The data scattering (i.e. the experimental standard deviation) is significantly lower then last year. The reason could be the lower volcanic activity of the volcano because the wind conditions are similar, as reported hereafter:

03 July 2008:
Sunny, wind: 15-20 kmh^{-1}, temperature: 10-15 °C.
04 July 2008:
Sunny, wind: 30-35 kmh^{-1}, temperature: 8-10 °C.
05 July 2008:
Sunny, wind: 30-40 kmh^{-1}, temperature: 8-10 °C.

10 July 2009:
Sunny, wind: 30-40 kmh^{-1}, temperature: 10-15 °C.

Table 4.3.3. Measurement uncertainty in Montagnola

Influence parameters, x_i	Value	Unit	u_i or a_i	Type A, s_i	Type B, a_i	Correction Δg	Type of distribution	Equivalent variance	Sensitivity coefficients	Contribution to the variance	Degrees of freedom, ν_i	Equivalent standard uncertainty
Instrument uncertainty		$m \cdot s^{-2}$	3.8E-08	3.8E-08				1.5E-15	1.00E+00	1.5E-15	19	3.8E-08
Coriolis effect		$m \cdot s^{-2}$	2.9E-08		2.9E-08		rectangular	2.8E-16	1.00E+00	2.8E-16	10	1.7E-08
Floor recoil effect			negligible									
Barometric pressure correction	4.3E-08	$m \cdot s^{-2}$	1.0E-08		1.0E-08	4.3E-08	rectangular	3.3E-17	1.00E+00	3.3E-17	15	5.8E-09
Tide correction	-3.6E-07	$m \cdot s^{-2}$	3.0E-09	3.0E-09		-3.6E-07		9.0E-18	1.00E+00	9.0E-18	15	3.0E-09
Ocean loading correction		$m \cdot s^{-2}$	2.0E-09	2.0E-09				4.0E-18	1.00E+00	4.0E-18	15	2.0E-09
Polar motion correction	-4.0E-09	$m \cdot s^{-3}$	negligible			-4.0E-09						
Standard deviation of the mean value		$m \cdot s^{-2}$	2.8E-08	2.8E-08				7.8E-16	1.00E+00	7.8E-16	495	2.8E-08
					Corr.	**-3.2E-07**	**$m \cdot s^{-2}$**	**Variance**		**2.6E-15**	**$m^2 \cdot s^{-4}$**	
					Combined standard uncertainty, u					**5.1E-08**	**$m \cdot s^{-2}$**	
					Degrees of freedom, ν_{eff} (Welch-Satterthwaite formula)					**54**		
					Confidence level, p					**95%**		
					Coverage factor, k (calculated with t-Student)					**2.01**		
					Expanded uncertainty, $U = ku$					**1.0E-07**	**$m \cdot s^{-2}$**	
					Relative expanded uncertainty, $U_{rel} = U/g$					**1.0E-08**		

4.4 Pizzi Deneri

The observation station of Pizzi Deneri is located in a room of the Osservatorio “Pizzi Deneri” (INGV), fig. 4.4.1 and 4.4.2.

The measurement was carried on 13-14 July 2009.

The position of the measurement point (fig. 4.4.3) referred to the room is showed on the plan of the building, fig. 4.4.4. The orientation of the instrument is showed by the red triangle where the black square represents the laser body.

The instrument processed and stored 989 trajectories.

The measured data are filtered by applying rejecting criteria. The most critical factor is the visibility variation of the interference signal during the trajectory, which highlights an horizontal motion of the test-body. The effect due to the Coriolis force and the beam share are minimized by rejecting those launches with a decrease of visibility bigger that 10%.

Outliers are found by applying the Chauvenet criterion to the estimating parameters such as the vertical gradient, the friction of residual air and to the estimated *g* value.

The final *g* value is obtained by averaging 192 trajectories. Table 4.4.1. reports the most important experimental results. Other information concerning the apparatus setup are reported in table 4.4.2.

The time series of the post-processed trajectories, data sets (each correspondent to the average of 50 launches) and trajectory residuals are reported in figure 4.4.5. The apparatus experienced an oscillation of about $\pm 6.0 \times 10^{-8}$ m·s^{-2}. The averaged trajectory residuals after the measurement session are within $\pm 1 \times 10^{-9}$ m.

The graphs reported in figure 4.4.6. represent the density frequency histograms and normal probability graphs of the *g* value, gradient and friction coefficient of the measurement session. The χ^2 test doesn’t reject the null hypothesis, i.e. the normal distribution, with a 80% confidence level.
Figure 4.4.7. reports ambient temperature, local barometric pressure and launch chamber pressure acquired at each launch and the applied tide corrections.

The measurement uncertainty is summarized in table 4.4.3. It includes the instrumental uncertainty reported in tab. 3.1.

Figure 4.4.1. Observation site at Pizzi Deneri

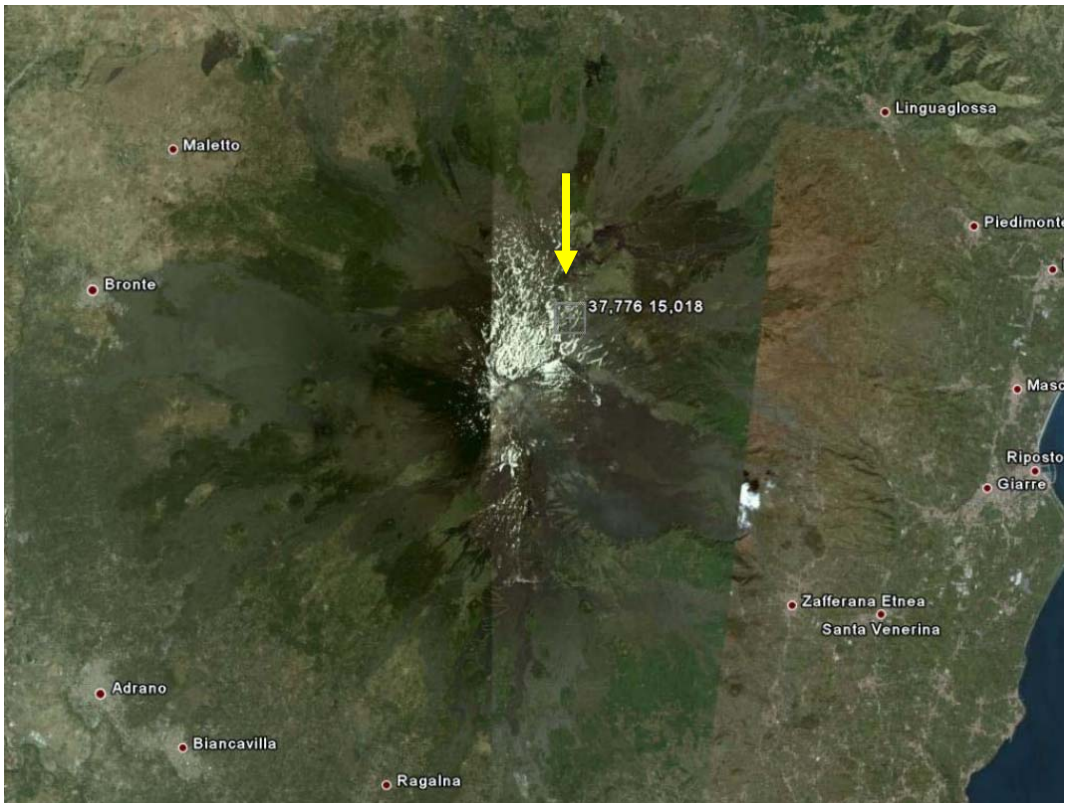

Figure 4.4.2. Satellite image of the observation site at Pizzi Deneri

Figure 4.4.3. Observation station at Pizzi Deneri

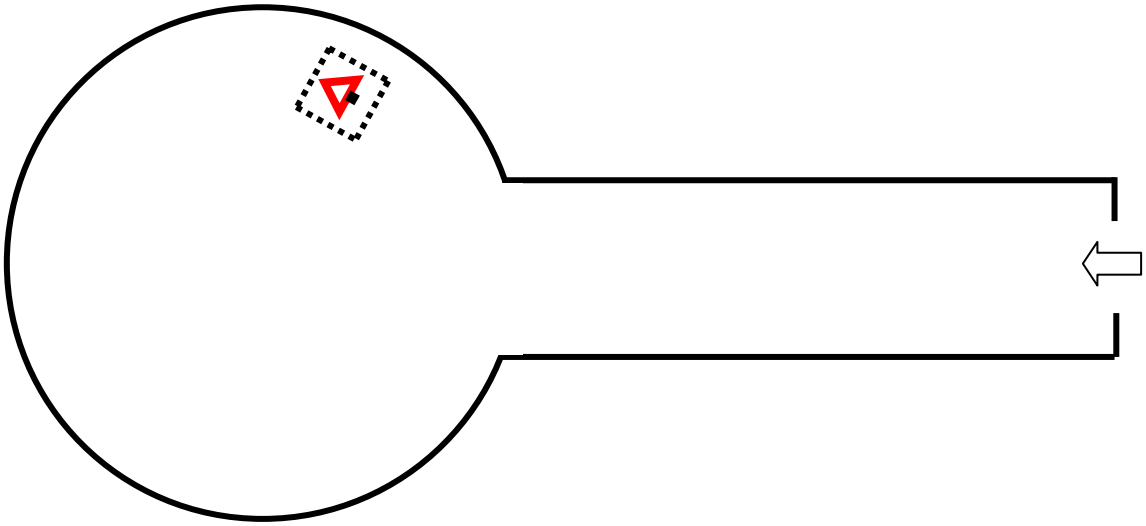

Figure 4.4.4. Plane of the building at Pizzi Deneri

Table 4.4.1. Experimental results in Pizzi Deneri

Observation Station: **Pizzi Deneri**	
Observation start (data and time in UTC)	2009/07/13 14:50:29
Observation stop (data and time in UTC)	2009/07/14 09:25:42
Geodetic longitude	λ = 15.0180°
Geodetic latitude	φ = 37.7660°
Topographic elevation	H_T = 2820 m
Nominal pressure at the observation site	P_N = 717.3 mbar
Pole coordinates in IERS system	x = 0.171964", y = 0.522364"
Measurement parameters	
Total observation time	T_m = 18.59 h
Measurement rate	m_r = 82 h^{-1}
Total processed and stored throws	n_{ps} = 989
Temperature range	T = (12.1 ÷ 14.2)°C
Local barometric pressure (mean)	P = 733.6 mbar
χ^2 test (80% confidence level)	χ^2_{max} = 21.1; χ^2_{min} = 7.8; χ^2_{exp} = 10.9
Corrections	
Laser beam verticality	Δg_{bv} = +0.6 × 10^{-8} m·s^{-2}
Laser beam divergence	Δg_{bd} = +10.9 × 10^{-8} m·s^{-2}
Overall drift	Δg_d = +22.6 × 10^{-8} m·s^{-2}
Polar motion	Δg_{pm} = -0.6 × 10^{-8} m·s^{-2}
Tide and ocean loading (mean)	Δg_{tol} = -4.2 × 10^{-8} m·s^{-2}
Local barometric pressure (mean)	Δg_{bp} = +4.9 × 10^{-8} m·s^{-2}
Results	
corrected mean *g* value	**g_{mv} = 979 379 869.1 × 10^{-8} m·s^{-2}**
Reference height	**h_{ref} = 489.7 mm**
Number of throws accepted for the average	**n = 192**
Experimental standard deviation	s_g = 167 × 10^{-8} m·s^{-2}
Experimental standard deviation of the mean value	**s_{gm} = 12.0 × 10^{-8} m·s^{-2}**
Measurement combined uncertainty	u_{gm} = 12.7 × 10^{-8} m·s^{-2}
Measurement expanded uncertainty (p = 95%, ν = 217, k = 1.97)	**U_{gm} = 25.1 × 10^{-8} m·s^{-2}**
Vertical gradient	γ = (378.8 ± 19.3) × 10^{-8} s^{-2}

Table 4.4.2. Apparatus setup in Pizzi Deneri

Instrument orientation	See fig. 4.4.4.
Fitting Model	Laser mod. & ground vibr. (19.3 Hz)
Fringe visibility threshold	f_{vt} = 10%
Measurements each set	n_{ma} = 50
Waveform digitizer sampling frequency	S_f = 50 MHz
Laser wavelength	λ_l = 632.9912130 × 10^{-9} m
Clock frequency	f_c = 10000000.0075 Hz
Vertical gradient input	γ = 0.000002700 s^{-2}
Rise station number	n_{rs} = 350
Leaved upper stations	n_{sl} = 2
Laser modulation frequency	f_{lm} = 1165.2 Hz

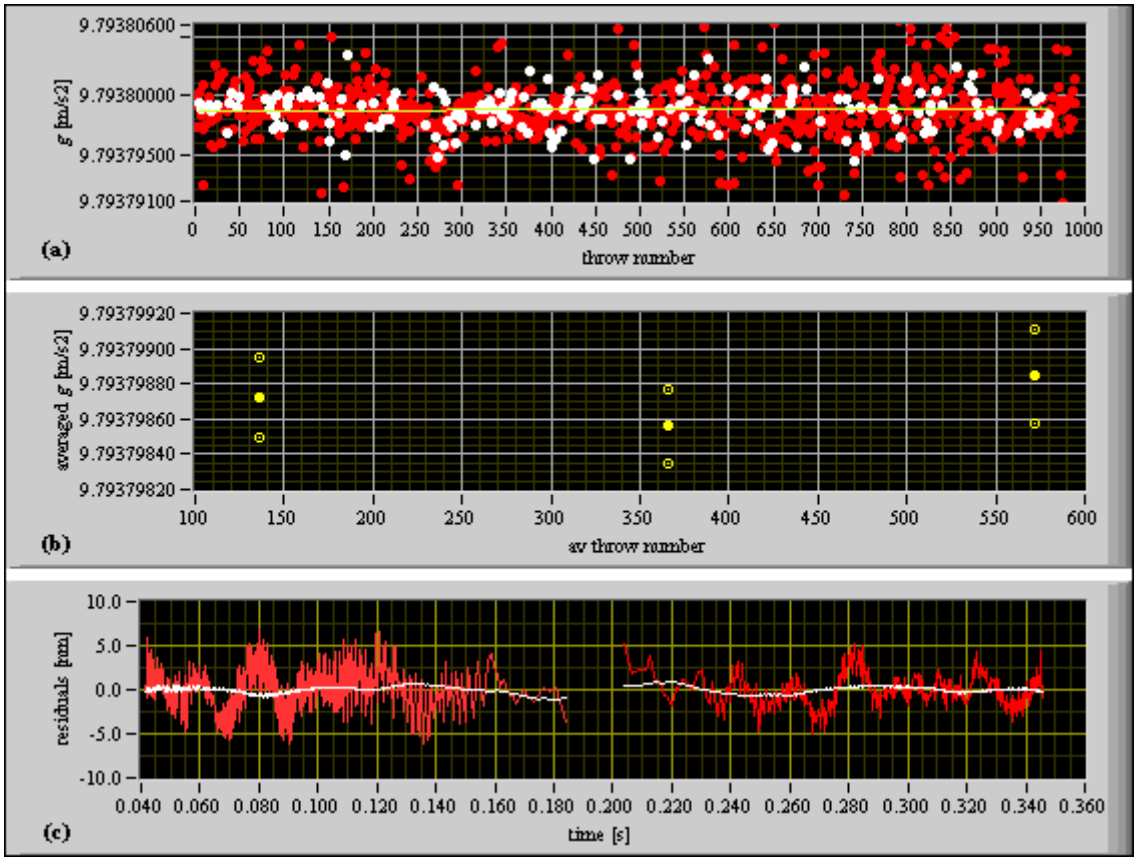

Figure 4.4.5. Time series (rejected-red, accepted-white) (a), Data sets (average of 50 launches) (b), trajectory residuals (one launch-red, average-white) (c) at Pizzi Deneri

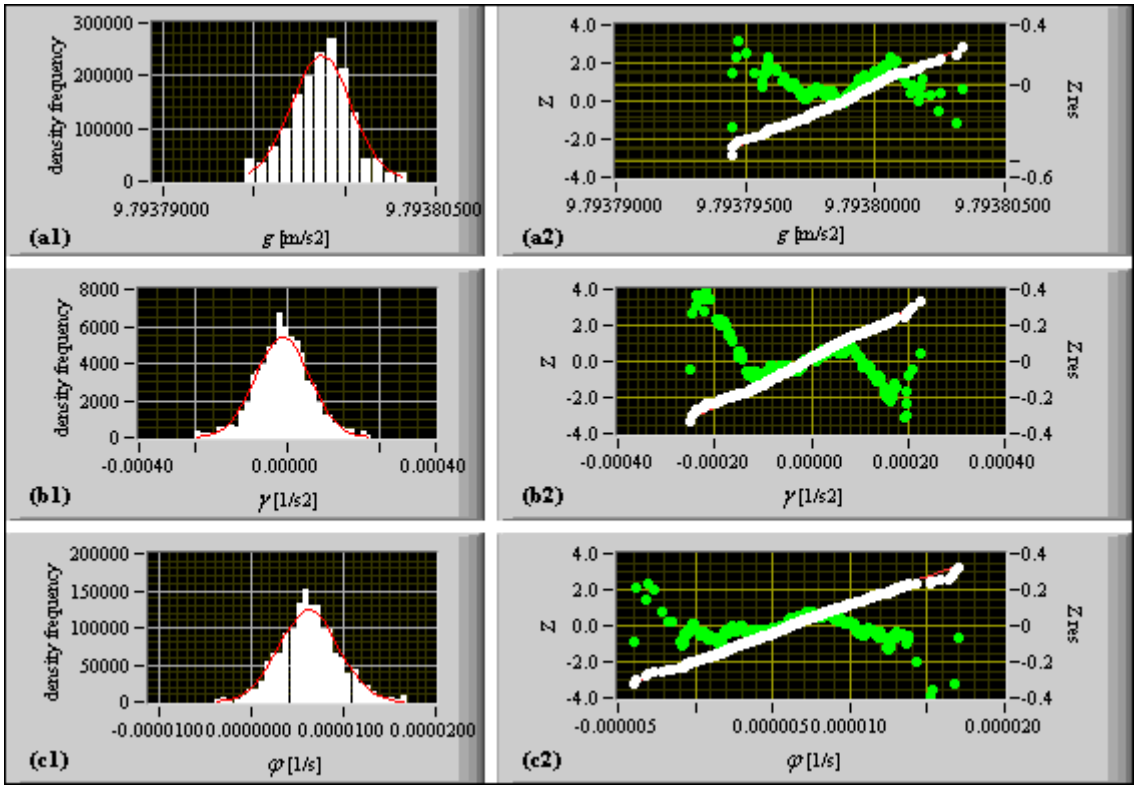

Figure 4.4.6. Density frequency graphs (1) and normal probability graphs (2) of the *g* value (a), gradient (b) and friction coefficient (c) measured at Pizzi Deneri

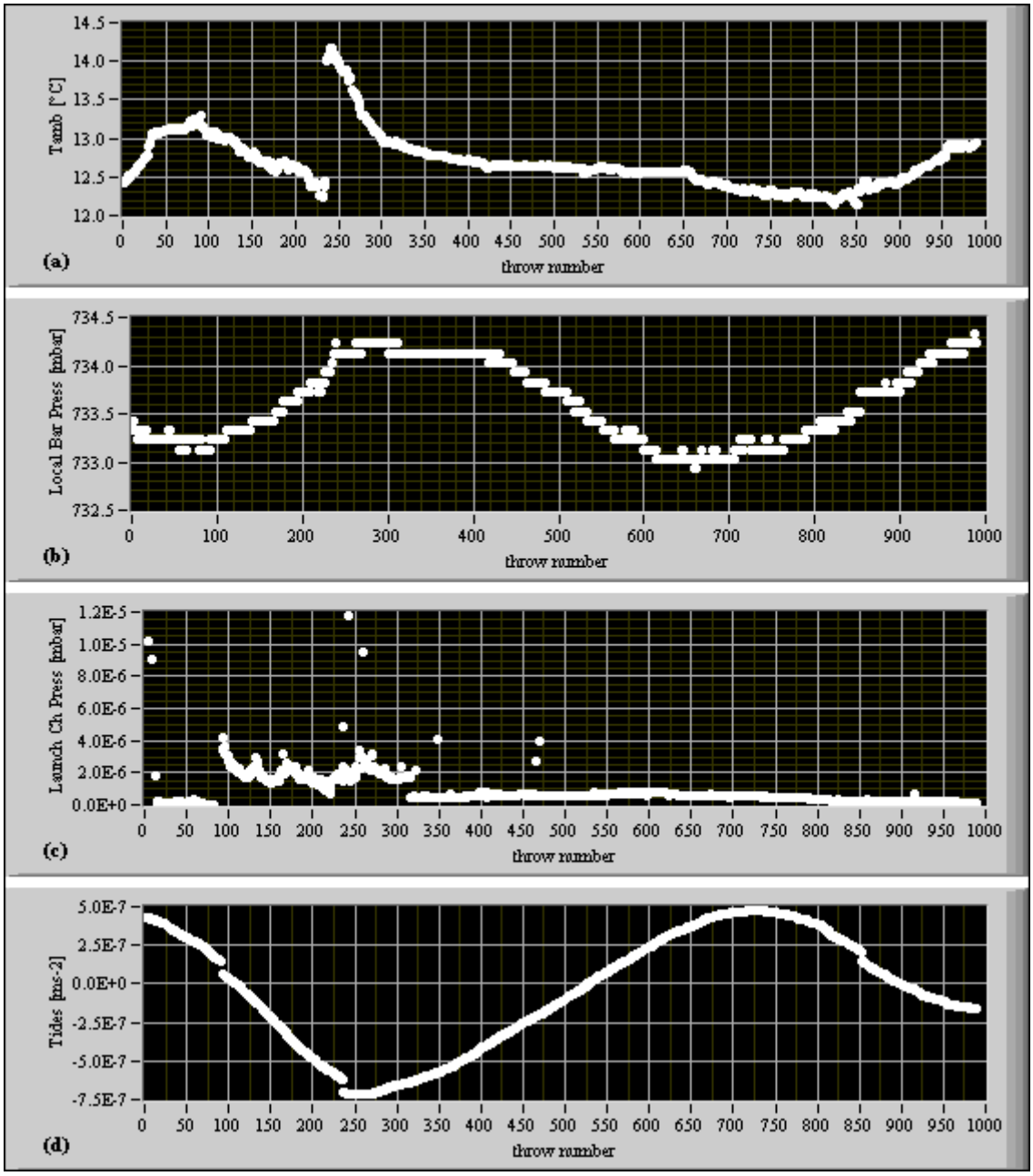

Figure 4.4.7. Ambient temp. (a), local barometric pressure (b) and launch chamber pressure (c) acquired at each launch and applied tide corrections (d) at Pizzi Deneri

Remarks

During the measurement session the overall drift was $+22.6 \times 10^{-8}$ ms^{-2}. The trajectory was reconstructed with the model that takes into account the laser modulation and the vibration of the inertial system. The best results were obtained by removing the 2 upper stations from the fit. The average of the trajectory residuals shows that the floor is really stiff but the scattering of the data highlights that the observation site is not quite.

The measurements of the free-fall acceleration are considered to be correct within the evaluated uncertainty.

Table 4.4.3. Measurement uncertainty at Pizzi Deneri

Influence parameters, x_i	Value	Unit	u_i or a_i	Type A, s_i	Type B, a_i	Correction Δg	Type of distribution	Equivalent variance	Sensitivity coefficients	Contribution to the variance	Degrees of freedom, ν_i	Equivalent standard uncertainty
Instrument uncertainty		$m \cdot s^{-2}$	3.8E-08	3.8E-08				1.5E-15	1.00E+00	1.5E-15	19	3.8E-08
Coriolis effect		$m \cdot s^{-2}$	2.9E-08		2.9E-08		rectangular	2.8E-16	1.00E+00	2.8E-16	10	1.7E-08
Floor recoil effect			negligible									
Barometric pressure correction	2.9E-08	$m \cdot s^{-2}$	1.0E-08		1.0E-08	2.9E-08	rectangular	3.3E-17	1.00E+00	3.3E-17	15	5.8E-09
Tide correction	-4.2E-08	$m \cdot s^{-2}$	3.0E-09	3.0E-09		-4.2E-08		9.0E-18	1.00E+00	9.0E-18	15	3.0E-09
Ocean loading correction		$m \cdot s^{-2}$	2.0E-09	2.0E-09				4.0E-18	1.00E+00	4.0E-18	15	2.0E-09
Polar motion correction	-6.0E-09	$m \cdot s^{-3}$	negligible			-6.0E-09						
Standard deviation of the mean value		$m \cdot s^{-2}$	1.2E-07	1.2E-07				1.4E-14	1.00E+00	1.4E-14	191	1.2E-07
					Corr.	**-1.9E-08**	**$m \cdot s^{-2}$**	**Variance**		**1.6E-14**	**$m^2 \cdot s^{-4}$**	
					Combined standard uncertainty, u					**1.3E-07**	**$m \cdot s^{-2}$**	
					Degrees of freedom, ν_{eff} (Welch-Satterthwaite formula)					**217**		
					Confidence level, p					**95%**		
					Coverage factor, k (calculated with t-Student)					**1.97**		
					Expanded uncertainty, $U = ku$					**2.5E-07**	**$m \cdot s^{-2}$**	
					Relative expanded uncertainty, $U_{rel} = U/g$					**2.6E-08**		

4.5 Piano Provanzana

The observation station of Piano Provenzana is located in a building of the arrive station of the cabin-lift, fig. 4.5.1 and 4.5.2.

The measurement was carried on 11-12 July 2009.

The position of the measurement point (fig. 4.5.3) referred to the room is showed on the plan of the building, fig. 4.5.4. The orientation of the instrument is showed by the red triangle where the black square represents the laser body.

The instrument processed and stored 999 trajectories.

The measured data are filtered by applying rejecting criteria. The most critical factor is the visibility variation of the interference signal during the trajectory, which highlights an horizontal motion of the test-body. The effect due to the Coriolis force and the beam share are minimized by rejecting those launches with a decrease of visibility bigger that 10%.

Outliers are found by applying the Chauvenet criterion to the estimating parameters such as the vertical gradient, the friction of residual air and to the estimated *g* value.

The final *g* value is obtained by averaging 192 trajectories. Table 4.5.1. reports the most important experimental results. Other information concerning the apparatus setup are reported in table 4.5.2.

The time series of the post-processed trajectories, data sets (each correspondent to the average of 50 launches) and trajectory residuals are reported in figure 4.5.5. The apparatus experienced an oscillation of about $\pm 5.0 \times 10^{-8}$ m·s^{-2}. The averaged trajectory residuals after the measurement session are within $\pm 5 \times 10^{-9}$ m.

The graphs reported in figure 4.5.6. represent the density frequency histograms and normal probability graphs of the *g* value, gradient and friction coefficient of the measurement session. The χ^2 test doesn't reject the null hypothesis, i.e. the normal distribution, with a 80% confidence level.
Figure 4.5.7. reports ambient temperature, local barometric pressure and launch chamber pressure acquired at each launch and the applied tide corrections.

The measurement uncertainty is summarized in table 4.5.3. It includes the instrumental uncertainty reported in tab. 3.1.

Figure 4.5.1. Observation site in Piano Provenzana

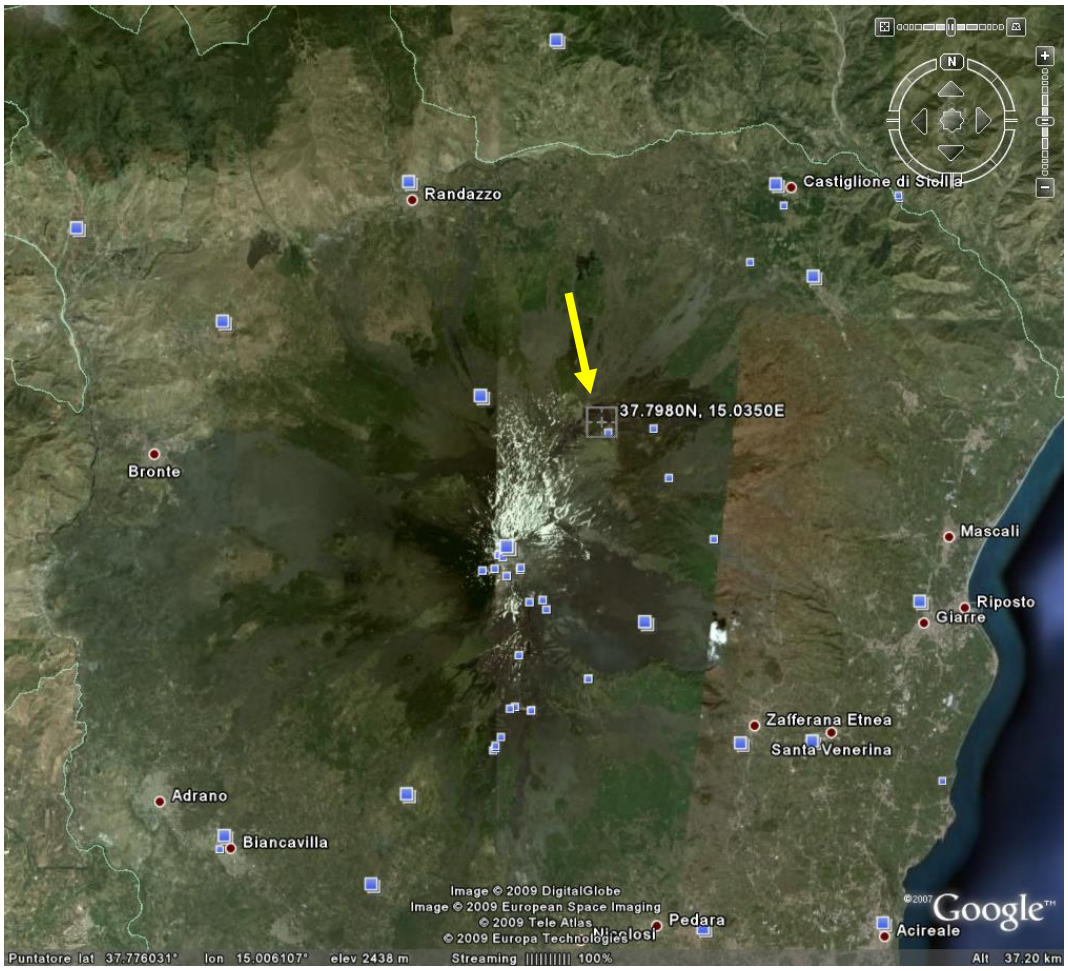

Figure 4.5.2. Satellite image of the observation site in Piano Provenzana

Figure 4.5.3. Observation station in Piano Provenzana

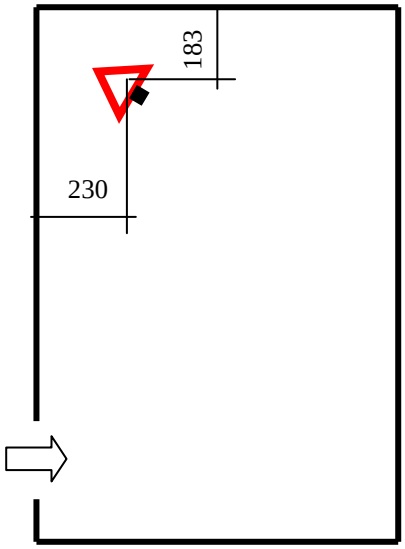

Figure 4.5.4. Plane of the building in Piano Provenzana

Table 4.5.1. Experimental results in Piano Provenzana

Observation Station: **Piano Provenzana**	
Observation start (data and time in UTC)	2009/07/11 15:18:33
Observation stop (data and time in UTC)	2009/07/12 04:20:27
Geodetic longitude	λ = 15.0350°
Geodetic latitude	φ = 37.7980°
Topographic elevation	H_T = 1825 m
Nominal pressure at the observation site	P_N = 812.4 mbar
Pole coordinates in IERS system	x = 0.165862", y = 0.52423"
Measurement parameters	
Total observation time	T_m = 13.03 h
Measurement rate	m_r = 87 h^{-1}
Total processed and stored throws	n_{ps} = 999
Temperature range	T = (17.8 ÷ 18.5)°C
Local barometric pressure (mean)	P = 822.0 mbar
χ^2 test (80% confidence level)	χ^2_{max} = 23.5; χ^2_{min} = 9.3; χ^2_{exp} = 14.1
Corrections	
Laser beam verticality	Δg_{bv} = +0.6 × 10^{-8} m·s^{-2}
Laser beam divergence	Δg_{bd} = +10.9 × 10^{-8} m·s^{-2}
Overall drift	Δg_d = +24.9 × 10^{-8} m·s^{-2}
Polar motion	Δg_{pm} = -0.4 × 10^{-8} m·s^{-2}
Tide and ocean loading (mean)	Δg_{tol} = -21.9 × 10^{-8} m·s^{-2}
Local barometric pressure (mean)	Δg_{bp} = +2.9 × 10^{-8} m·s^{-2}
Results	
corrected mean *g* value	**g_{mv} = 979 618 347.9 × 10^{-8} m·s^{-2}**
Reference height	**h_{ref} = 497.5 mm**
Number of throws accepted for the average	**n = 246**
Experimental standard deviation	s_g = 48.0 × 10^{-8} m·s^{-2}
Experimental standard deviation of the mean value	**s_{gm} = 3.0 × 10^{-8} m·s^{-2}**
Measurement combined uncertainty	u_{gm} = 5.2 × 10^{-8} m·s^{-2}
Measurement expanded uncertainty (p = 95%, ν = 217, k = 1.97)	**U_{gm} = 10.4 × 10^{-8} m·s^{-2}**
Vertical gradient	γ = (258.7 ± 16.7) × 10^{-8} s^{-2}

Table 4.5.2. Apparatus setup in Piano Provenzana

Instrument orientation	See fig. 4.5.4.
Fitting Model	Laser mod. & ground vibr. (13.2 Hz)
Fringe visibility threshold	f_{vt} = 10%
Measurements each set	n_{ma} = 50
Waveform digitizer sampling frequency	S_f = 50 MHz
Laser wavelength	λ_l = 632.9912130 × 10^{-9} m
Clock frequency	f_c = 10000000.0075 Hz
Vertical gradient input	γ = 0.000002700 s^{-2}
Rise station number	n_{rs} = 350
Leaved upper stations	n_{sl} = 2
Laser modulation frequency	f_{lm} = 1165.2 Hz

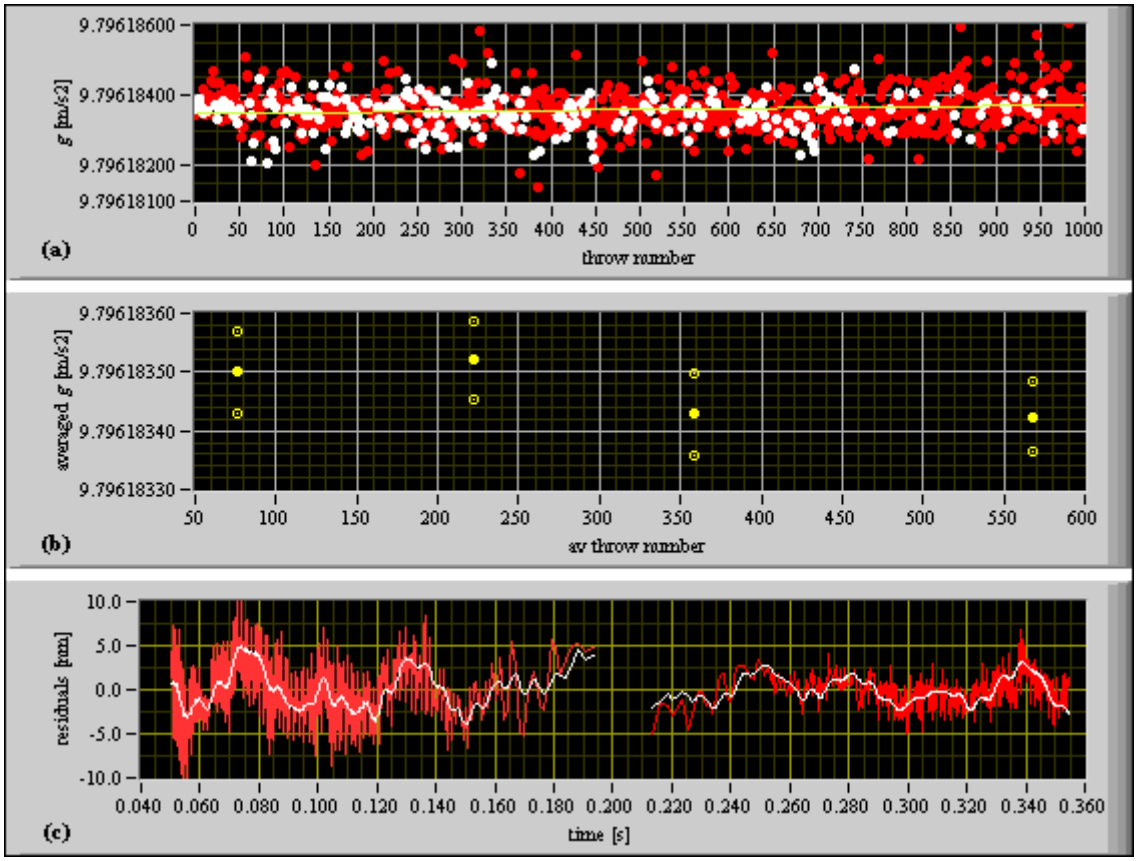

Figure 4.4.5. Time series (rejected-red, accepted-white) (a), Data sets (average of 50 launches) (b), trajectory residuals (one launch-red, average-white) (c) at Pizzi Deneri

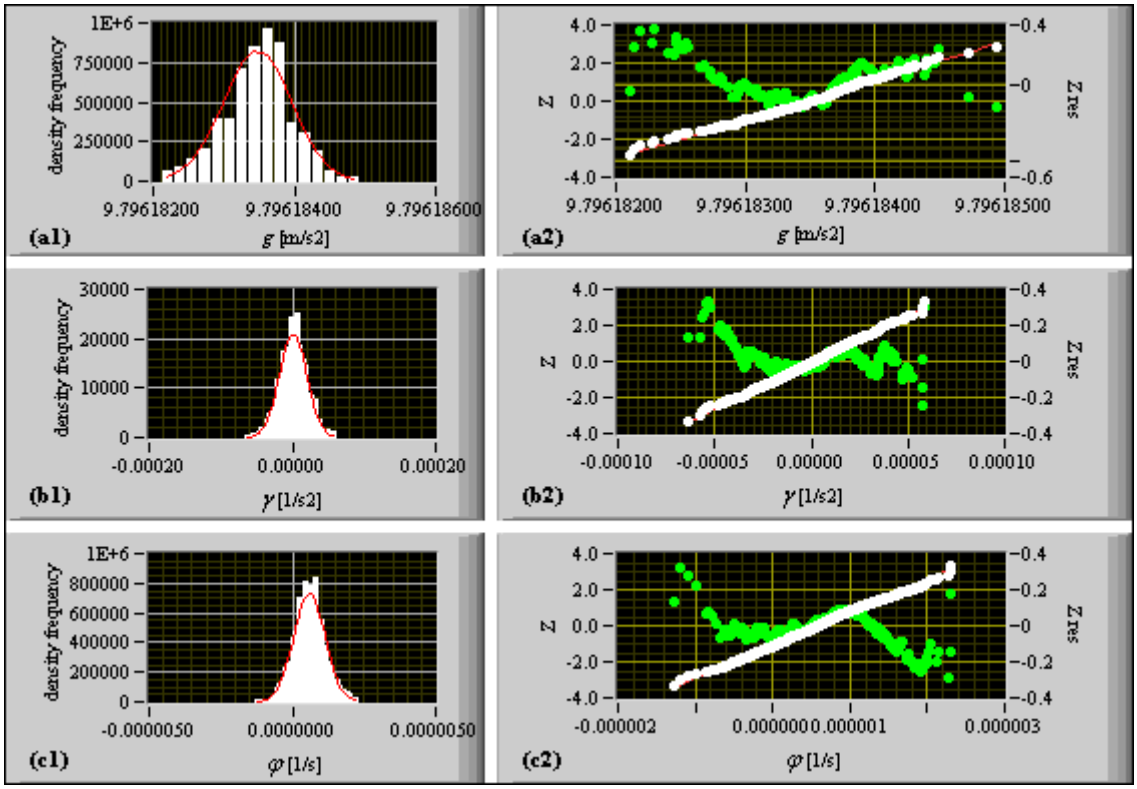

Figure 4.5.6. Density frequency graphs (1) and normal probability graphs (2) of the *g* value (a), gradient (b) and friction coefficient (c) measured in Piano Provenzana

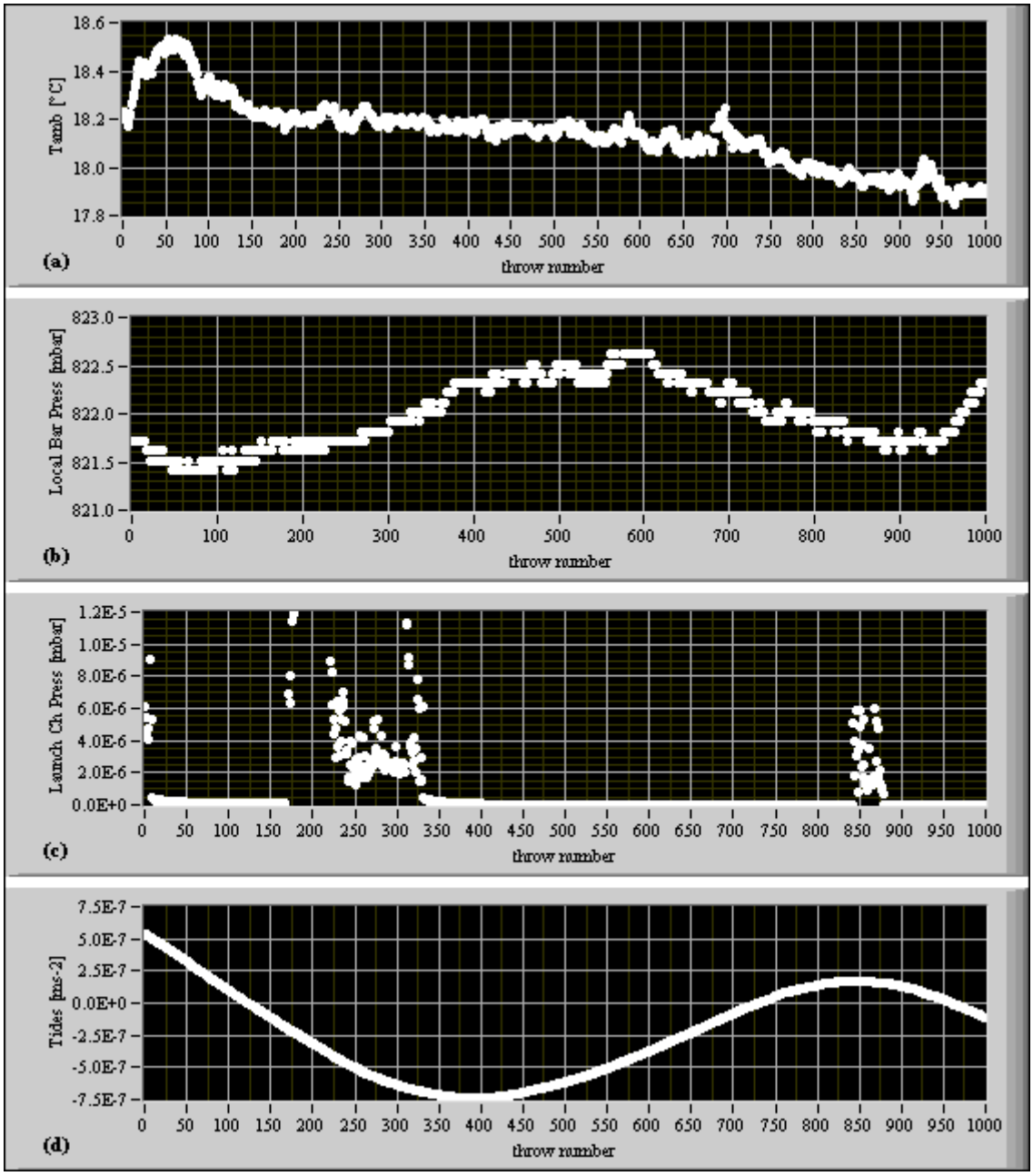

Figure 4.5.7. Ambient temp. (a), local barometric pressure (b) and launch chamber pressure (c) acquired at each launch and applied tide corrections (d) in Piano Provenzana

Remarks

During the measurement session the overall drift was $+24.9 \times 10^{-8}$ ms^{-2}. The trajectory was reconstructed with the model that takes into account the laser modulation and the vibration of the inertial system. The best results were obtained by removing the 2 upper stations from the fit. The average of the trajectory residuals shows that the floor is stiff and the scattering of the data highlights that the observation site is quite.

The measurements of the free-fall acceleration are considered to be correct within the evaluated uncertainty.

Table 4.5.3. Measurement uncertainty in Piano Provenzana

Influence parameters, x_i	Value	Unit	u_i or a_i	Type A, s_i	Type B, a_i	Correction Δg	Type of distribution	Equivalent variance	Sensitivity coefficients	Contribution to the variance	Degrees of freedom, ν_i	Equivalent standard uncertainty
Instrument uncertainty		$m \cdot s^{-2}$	3.8E-08	3.8E-08				1.5E-15	1.00E+00	1.5E-15	19	3.8E-08
Coriolis effect		$m \cdot s^{-2}$	2.9E-08		2.9E-08		rectangular	2.8E-16	1.00E+00	2.8E-16	10	1.7E-08
Floor recoil effect			negligible									
Barometric pressure correction	2.9E-08	$m \cdot s^{-2}$	1.0E-08		1.0E-08	2.9E-08	rectangular	3.3E-17	1.00E+00	3.3E-17	15	5.8E-09
Tide correction	-2.2E-07	$m \cdot s^{-2}$	3.0E-09	3.0E-09		-2.2E-07		9.0E-18	1.00E+00	9.0E-18	15	3.0E-09
Ocean loading correction		$m \cdot s^{-2}$	2.0E-09	2.0E-09				4.0E-18	1.00E+00	4.0E-18	15	2.0E-09
Polar motion correction	-4.0E-09	$m \cdot s^{-3}$	negligible			-4.0E-09						
Standard deviation of the mean value		$m \cdot s^{-2}$	3.0E-08	3.0E-08				9.0E-16	1.00E+00	9.0E-16	245	3.0E-08
					Corr.	**-1.9E-07**	**$m \cdot s^{-2}$**	**Variance**		**2.7E-15**	**$m^2 \cdot s^{-4}$**	
					Combined standard uncertainty, u					**5.2E-08**	**$m \cdot s^{-2}$**	
					Degrees of freedom, ν_{eff} (Welch-Satterthwaite formula)					**58**		
					Confidence level, p					**95%**		
					Coverage factor, k (calculated with t-Student)					**2.00**		
					Expanded uncertainty, $U = ku$					**1.0E-07**	**$m \cdot s^{-2}$**	
					Relative expanded uncertainty, $U_{rel} = U/g$					**1.1E-08**		

REFERENCES

[1] D'Agostino,G., "*Development and Metrological Characterization of a New Transportable Absolute Gravimeter*", PhD Thesis, 2005.

[2] Cerutti,G., Cannizzo,L., Sakuma,A., Hostache, J., "*A transportable apparatus for absolute gravity measurements*", In: VDI-Berichte n. 212, 1974: p. 49.

[3] Germak,A., Desogus,S., Origlia,C., "*Interferometer for the IMGC rise-and-fall absolute gravimeter*", In: Metrologia, Special issue on gravimetry, Bureau Int Poids Mesures, BIPM, Pavillon De Breteuil, F-92312, Sèvres Cedex, France, 2002, Vol. 39, Nr. 5, pp. 471-475.

[4] D'Agostino,G., Germak,A., Desogus,S., Barbato,G. "*A Method to Estimate the Time-Position Coordinates of a Free-Falling Test-Mass in Absolute Grvimetry*", In: Metrologia Vol. 42, No. 4, pp. 233-238, August 2005.

[5] "Guide to the Expression of Uncertainty in Measurement", BIPM, IEC, ISCC, ISO, IUPAC, IUPAP, OIML, ISO, 1993.